however, two markedly different features: the exons corresponding to human exons 2 and 3 are not identifiable, and exon 2, which by definition corresponds to human exon 4, is expanded (Fig. 2c). Reverse transcription (RT)-PCR analysis using primers S3 and AS2 (Fig. 2c) revealed that

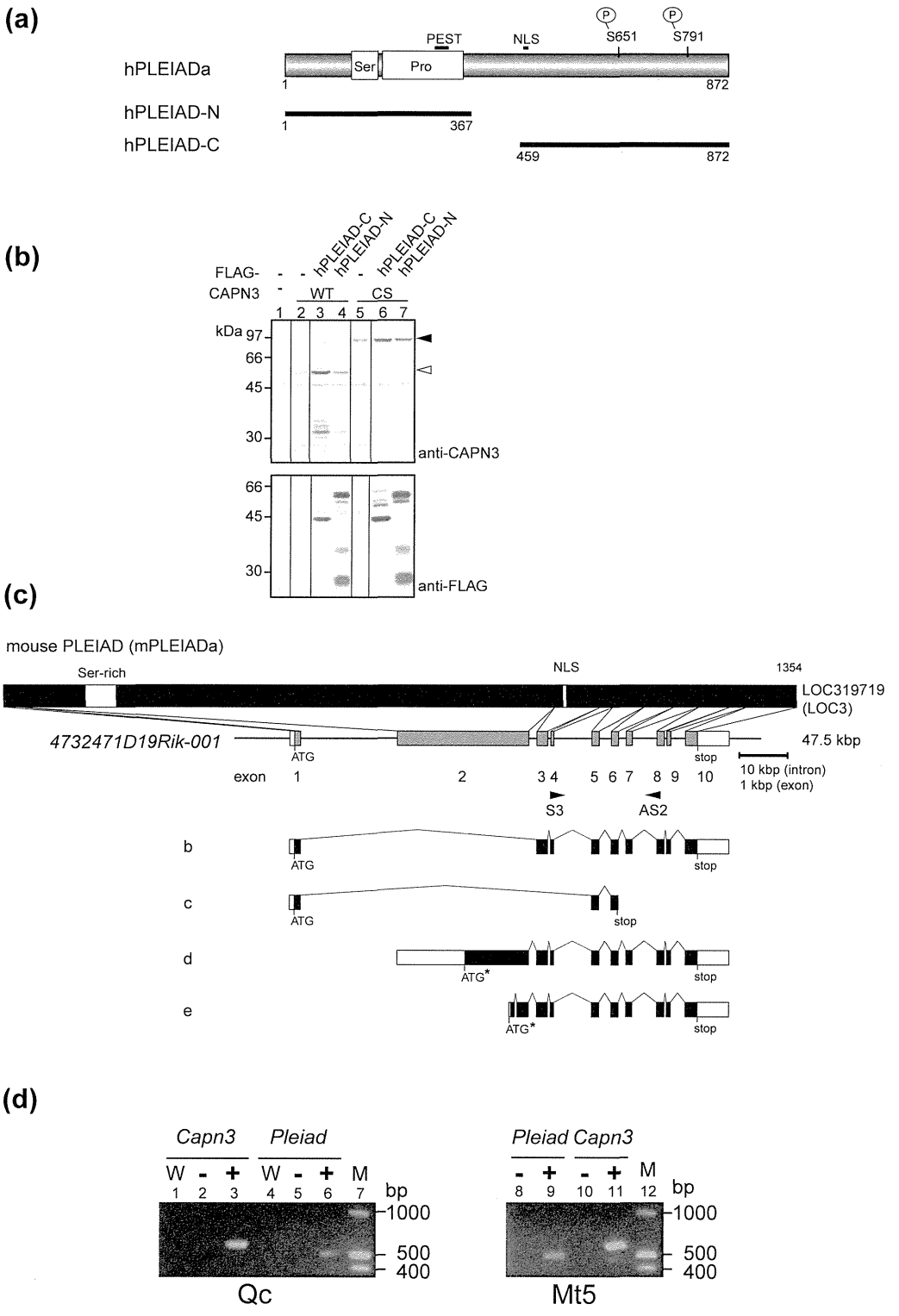


**Fig. 2** (*legend on previous page*)

**Table 1.** Primers used in this study for cDNA cloning and RT-PCR detection

| Primer | Reference sequence no. | Position[a] | Sequence |
|---|---|---|---|
| S1 | BC037298 | 143–159s | cggtcggtaCCCGyAGCCATGGAGGA[b] |
| S2 | | 417–439s | aacacatATGGCACCAGCATCTGCTTCTGG[b] |
| S3[c] | | 2071–2090s | TCACCTATGTCATGGAGGAA |
| AS1 | | 3065–3048as | GGAGAGAGAGTTCAGGAGG |
| AS2[c] | | 2545–2562as | GGTGGCTTTCCATGGTAG |
| AS3 | | 2155–2170as | AGGGTCTGCTGAAAGT |
| AS4 | | 739–759as | GGTCCAAATCTACAGGATCAC |
| CAPN3_411 | NM_000070.2 | 1801–1820s | CTCTT CACCA TTGGC TTCGC, |
| CAPN3_412 | | 2347–2367as | CAGGTCCTTGTGTTTGTTCAC |

[a] s, sense strand (5′ → 3′); as, antisense strand (5′ ← 3′).
[b] Lowercase letters indicate the sequence added or modified for cloning purposes.
[c] The sequences of these primers coincide with the corresponding mouse *Pleiad* sequences and, thus, were also used for amplification of mouse cDNA.

transcripts encoding the conserved C-terminal region of mPLEIADa are expressed in mouse skm cells (Fig. 2d, lanes 6 and 9).

A psi-BLAST homology search of databases using the human PLEIAD (hPLEIAD) sequence as a seed revealed significant conservation of the C-terminal half of hPLEIAD, corresponding approximately to exons 5–12 (hPLEIAD-C), among vertebrates (Fig. 2a and Tables 2 and 3). In contrast, the sequence of the N-terminal half of hPLEIAD, hPLEIAD-N, was not an efficient seed for retrieving a conserved structure among vertebrate PLEIAD homologs. These observations suggest that the regulation of CAPN3 autolysis was conducted by the C-terminal region of PLEIAD homologs during evolution.

## PLEIAD interacts with CTBP1, a potential CAPN3 substrate

Yeast two-hybrid (YTH) screening identified CTBP1 as an interacting protein candidate for PLEIAD. CTBP1 is a highly conserved transcriptional co-repressor, and its structure–function relationships have been well studied (Fig. 3a).[34] In addition to hPLEIADa, which was originally used as a bait construct for the screening, hPLEIADf also interacted with CTBP1 (data not shown). In contrast to PLEIAD's effect on CAPN3's autolysis, PLEIAD's N-terminal region was sufficient for its interaction with CTBP1 (Fig. 3b, column D).

To characterize the mechanism of the CTBP1–PLEIAD interaction, we examined mutations that have been shown to abrogate CTBP1's interaction with the PLDLS motif in target proteins (Fig. 3b, columns F and H). Examining two mutants, A52E and V66R, did not demonstrate the interaction with hPLEIADa, hPLEIAD-N, or hPLEIADf:ex4term (2F to 4F and 2H to 4H). Therefore, it is possible that the structure of CTBP1 critical for its formation of co-repressor complexes is also involved in its interaction with PLEIAD. On the other hand, mutations in NAD(H)-binding domain of CTBP1 caused autoactivation of

**Table 2.** Amino acid sequences of PLEIAD homologs used in this study

| Species (abbreviation) | General name | Accession no.[a] | Size (aa) | Homologous region[b] (aa) |
|---|---|---|---|---|
| *Homo sapiens* (*H. s.*) | Human | Q8NDZ2 | 872 | 459–872 |
| *Mus musculus* (*M. m.*) | Mouse | NP_795961.3 | 1354 | 945–1354 |
| *Bos taurus* (*B. t.*) | Bovine | XP_002690456.1 | 451 | 44–451 |
| *M. domestica* (*M. d.*) | Opossum | XP_001380898.1 | 865 | 461–865 |
| *Gallus gallus* (*G. g.*) | Chicken | XP_414554.1 | 646 | 245–646 |
| *Taeniopygia guttata* (*T. g.*) | Zebra finch | XP_002194388.1 | 605 | 210–605 |
| *Meleagris gallopavo* (*M. g.*) | Turkey | XP_003210405.1[c] (ENSMGAT00000005306) | 433 | 32–433 |
| *Anolis carolinensis* (*A. c.*) | Green anole lizard | XP_003227968.1[c] (ENSACAT00000006428) | 441 | 47–441 |
| *Xenopus tropicalis* (*X. t.*) | Western clawed frog | XP_002938112.1[c] (NW_003163664, ENSXETT00000064005, EL834443) | 587 | 215–587 |
| *Oreochromis niloticus* (*O. n.*) | Cichlid fish | XP_003455259.1[c] (NT_167549) | 426 | 43–426 |
| *Tetraodon nigroviridis* (*T. n.*) | Puffer fish | CAF92416[c,d] (CAAE01009900) | 316 | 54–316 |
| *Danio rerio* (*D. r.*) | Zebra fish | XP_001922583.1[c] (ENSDART00000129265) | 770 | 381–770 |

[a] Data were retrieved from NCBI and Ensembl databases.
[b] Amino acid sequences corresponding to those encoded by exons 5–12 (459–872) in the human C5orf25 gene were used for analysis.
[c] The sequence was revised using genomic and EST sequences shown in parentheses.
[d] Gaps were left unfiled in consideration of uncertainty of deposited genome sequences.

**Table 3.** Identity and similarity among 12 vertebrate PLEIAD sequences

| % Identity | Mammals | | | | Birds | | | Reptile | Amphibian | Fish | | |
|---|---|---|---|---|---|---|---|---|---|---|---|---|
| % Similarity | *H. s.* | *M. m.* | *B. t.* | *M. d.* | *G. g.* | *T. g.* | *M. g.* | *A. c.* | *X. t.* | *O. n.* | *T. n.*[a] | *D. r.* |
| *H. s.* | | 93.1 | 92.9 | 70.4 | 51.0 | 47.2 | 48.8 | 46.7 | 41.2 | 33.2 | *43.2* | 36.1 |
| *M. m.* | 99.0 | | 89.7 | 70.4 | 51.0 | 46.9 | 50.0 | 46.2 | 41.0 | 33.5 | *35.9* | 36.6 |
| *B. t.* | 99.5 | 99.0 | | 69.4 | 50.2 | 46.5 | 49.5 | 45.9 | 40.5 | 33.5 | *37.5* | 36.1 |
| *M. d.* | 91.0 | 91.5 | 91.0 | | 50.3 | 47.3 | 50.5 | 44.6 | 38.4 | 34.3 | *38.5* | 34.5 |
| *G. g.* | 84.4 | 83.9 | 84.2 | 84.5 | | 65.9 | 91.3 | 50.6 | 41.1 | 33.9 | *35.8* | 34.0 |
| *T. g.* | 82.0 | 82.0 | 81.8 | 81.8 | 90.0 | | 66.8 | 47.0 | 40.7 | 33.3 | *30.3* | 35.0 |
| *M. g.* | 82.2 | 83.2 | 83.2 | 83.5 | 98.0 | 89.8 | | 49.6 | 41.4 | 33.9 | *37.9* | 35.0 |
| *A. c.* | 79.7 | 79.4 | 78.9 | 81.0 | 82.0 | 80.5 | 82.5 | | 39.7 | 31.5 | *33.9* | 32.6 |
| *X. t.* | 75.0 | 75.8 | 75.3 | 78.0 | 76.1 | 76.7 | 76.1 | 75.6 | | 31.3 | *29.0* | 30.4 |
| *O. n.* | 73.1 | 73.4 | 73.4 | 72.6 | 70.8 | 70.5 | 72.0 | 70.8 | 76.5 | | *46.8* | 53.2 |
| *T. n.* | *77.3* | *72.6* | *77.3* | *74.0* | *70.5* | *68.1* | *72.6* | *71.4* | *71.0* | *79.9* | | *39.5* |
| *D. r.* | 72.8 | 73.5 | 72.0 | 75.5 | 73.0 | 74.1 | 72.9 | 74.7 | 79.3 | 85.8 | *81.5* | |

Species names are abbreviated as in Table 2.
[a] The values for the *T. nigroviridis* sequence are shown in italics since this sequence contains three gaps.

the prey plasmid and were not competent for the analysis using YTH system.

Unlike the interaction between CAPN3 and PLEIAD, the interaction between CTBP1 and PLEIAD and/or CAPN3 was not detectable using protein expression in COS7 cells. To ensure the presence of excess amount of CTBP1, we performed *in vitro* cotranslation of PLEIAD and CAPN3:CS in the presence of CTBP1 using cell-free protein expression system (Fig. 3c). Both PLEIADa and PLEIADf together with CTBP1 were coimmunoprecipitated by anti-CAPN3 (Fig. 3d, lanes 5 and 7). In contrast to PLEIAD, the amount of CTBP1 in immunoprecipitate was very small and the efficiency was quite low considering its abundant presence in "Input" (lanes 1–4).

Unexpectedly, the expression of CAPN3:WT in COS7 cells caused a significant decrease in endogenous CTBP1 (Fig. 4a, lane 3, gray arrowhead). This decrease was even more pronounced when the triple-tagged CTBP1 construct, MYC-CTBP1-EGFP-FLAG, was coexpressed with CAPN3:WT (Fig. 4a, lane 1). The detected major proteolytic fragment size (open arrow), ca 35 kDa, was larger than that calculated for EGFP with FLAG, ca 30 kDa, indicating that proteolysis by coexpressed CAPN3 occurred within CTBP1 and not in the tag regions. A splicing variant of mouse CAPN3, CAPN3:ΔIS1,[35] also resulted in the proteolysis of coexpressed CTBP1 (Fig. 4b, lane 4). As summarized at the bottom of Fig. 4b, the proteolysis of CTBP1 occurred in parallel with that of other potential CAPN3 substrates identified in COS7 cells, such as calpastatin and fodrin. The C-terminal proteolyzed fragment was purified by anti-FLAG immunoprecipitation, and its N-terminal sequence was determined to be $G^{410}$LPPVA by N-terminal sequencing (Fig. 4b, open arrow; data not shown).

We next examined if the proteolysis of endogenous CTBP1 in differentiated mouse skm primary cultured cells was induced upon the activation of CAPN3 by ouabain treatment, which increases the intracellular $Na^+$ and (indirectly) $Ca^{2+}$ concentrations.[32] The result was under our detection level (Fig. 4c, lane 2), suggesting that, unlike CAPN3 expressed in COS7 cells, substrate proteolysis by endogenous CAPN3 in skm is still tightly regulated even when its autolysis is detectable and/or the proteolysis of endogenous CTBP1 does not occur at a level that is artificially induced by CAPN3 overexpression in COS7 cells.

The effect of missense mutations that have been shown to compromise complex formation activities of CTBP1 on its property as a substrate for CAPN3 was also examined. Except for the mutation A52E, these mutations altered the susceptibility of CTBP1 to CAPN3-mediated proteolysis while the decrease in the amount of the proteolyzed fragment was observed.

These results suggest that PLEIAD has at least two functions mediated by different regions of the molecule: the N-terminal region recruits CTBP1, a substrate for CAPN3, and the C-terminal region is involved in suppressing CAPN3's protease activity.

### CTBP1 is also a substrate for conventional calpains

To obtain insight into the role of calpains in the proteolysis of CTBP1, we examined the proteolysis of recombinant CTBP1 by recombinant conventional calpains *in vitro*. CTBP1 was proteolyzed by CAPN1 + CAPNS1 (also called μ-calpain, abbreviated as "CAPN1/S1" in Fig. 5a, lanes 3 and 4) and CAPN2/S1 (m-calpain; data not shown). The specificity of the reaction was shown by the suppression

of most of the proteolysis in the presence of calpastatin (Fig. 5a, lane 5) or in the absence of $Ca^{2+}$ (lane 6). In parallel, reactions carried out in the presence (sample in lane 4) or absence (sample in lane 6) of $Ca^{2+}$ were analyzed by mass spectrometry to determine the sequences of proteolyzed

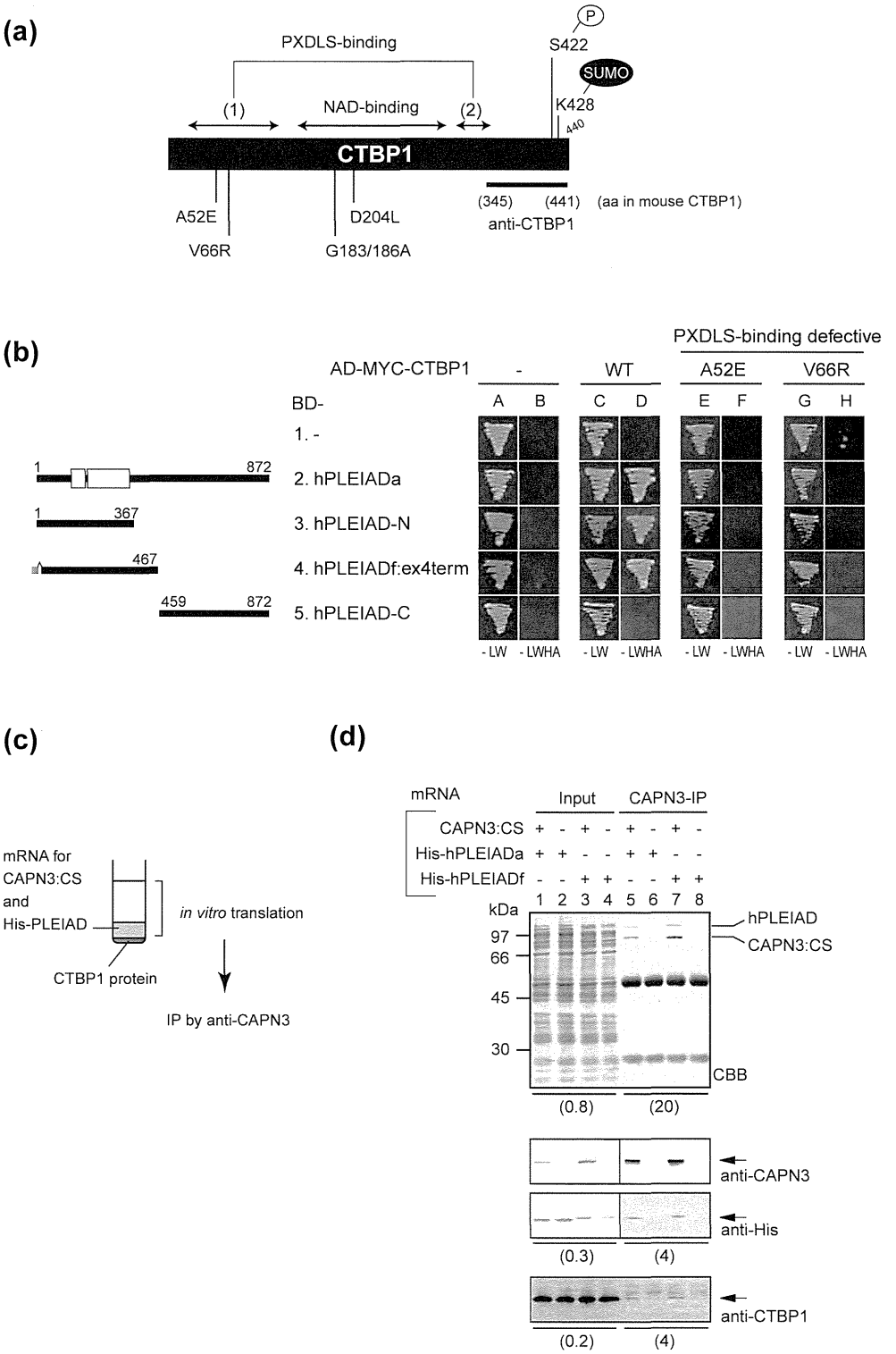


**Fig. 3** (*legend on next page*)

fragments. With >99% confidence, four peptides were identified in the [+$Ca^{2+}$] sample [Fig. 5b, (i) to (iv)], two of which [Fig. 5b, (iii) and (iv)] were also detectable in the [−$Ca^{2+}$] sample. These findings suggested that CTBP1 is cleaved at the N-termini of G376 (Fig. 5b, [1]) and V388 (Fig. 5b, [2]) by CAPN1 + S1 in the presence of $Ca^{2+}$.

As mentioned above, CAPN3 proteolyzed CTBP1 at Gly410 at the N-terminus (Fig. 4c). Therefore, the same position detected here (Fig. 5b, [4]) is very likely to be a proteolytic site for conventional calpain, as well. However, the possibility of nonspecific proteolysis by non-calpain contaminating proteases cannot be completely eliminated due to the detection of the same peptides in the [−$Ca^{2+}$] sample, although their intensity was much lower than that detected in the [+$Ca^{2+}$] sample. In addition, analysis of the CTBP1 sequence using our cleavage site predictor for calpain[36] recognized the three positions [1], [2], and [4] by three different algorithms (Fig. 5c). Collectively, these data indicate that sites [1], [2], and [4] are probably cleaved by conventional calpain and that site [3] may represent nonspecific proteolysis. It remains unclear whether cleavage sites [1] and [2] are recognized by CAPN3. However, the small amount of a fragment detectable above the major proteolyzed fragments in Fig. 4b (lanes 2 and 4, gray arrow) may indicate that the cleavage by CAPN3 also occurred at sites [1] and/or [2].

### PLEIAD may regulate CAPN3 that is not bound to sarcomere components

To gain further insight into PLEIAD's physiological relevance, we examined PLEIAD's cellular localization in primary cultures of chick skeletal myotubes expressing EGFP-hPLEIADf (Fig. 6). In total, 200 transfected cells expressing EGFP-hPLEIADf were compared to 150 cells expressing EGFP alone. In ~10% of the transfected cells, hPLEIADf was localized in a striated pattern within the sarcomeric I band, but most cells showed diffuse cytoplasmic staining (Fig. 6d, inset: see GFP staining, i.e., hPLEIADf, on each side of the Z-line, marked by staining for α-actinin). These results suggested that PLEIAD's primary target may be a population of CAPN3 that exists in the cytosol. For unknown reasons, it was more difficult to express EGFP-hPLEIADa as efficiently as EGFP-hPLEIADf. These two isoforms also showed different expression/degradation patterns in COS7 cells, independent of CAPN3's protease activity (Fig. 1d, lanes 4 and 5 and lanes 8 and 9, anti-FLAG). Such a difference might be enhanced in skeletal myotubes, resulting in a more severe degradation of hPLEIADa than of hPLEIADf.

## Discussion

The unique properties of CAPN3 include its very rapid and exhaustive autolysis *in vitro* in protein expression systems and nonmuscle cultured cells (CAPN3 is stable in primary skm cells[21]) and its dependence on both $Na^{+}$ and $Ca^{2+}$ for its activation.[32] These phenomena have been studied mostly with respect to causative factors; for example, it has been shown that CAPN3-specific insertion sequences, IS1 and IS2, are required for autolytic events.[21,35,37] In contrast, it is unclear why CAPN3 remains intact in skm cells without undergoing autolysis. Surprisingly, in CAPN3:CS knockin mice, in which the endogenous wild-type CAPN3 (CAPN3:WT) is replaced by a protease-inactive mutant CAPN3:CS, the amount of CAPN3:CS protein detected in the skm cells and tissues is the same as in wild-type mice. Moreover, the presence of intact CAPN3 protein, that is, of either WT or the CS mutant, is sufficient to fulfill its function at the triad region, even when its protease activity is lacking.[18,19] These findings strongly suggest that, in addition to connectin/titin, which is a strong candidate for stabilizing and regulating CAPN3 in muscle sarcomeres, another mechanism is present to stabilize CAPN3, especially when it is not associated with sarcomeres.

As an approach to understanding the mechanism by which CAPN3 conducts diverse functions in

**Fig. 3.** The N-terminal region of PLEIAD interacts with CTBP1. (a) YTH screening using a human skm cDNA library identified CTBP1 as a binding protein for PLEIAD. The functional annotation for human CTBP1 is shown. Among previously validated missense mutants, four different mutants that compromised complex formation activities of CTBP1 were selected. The mouse sequence has an insertion of 1 aa at the C-terminal region and therefore consists of 441 aa. Horizontal bar indicates the antigenic polypeptides for anti-CTBP1. (b) The N-terminal region, hPLEIAD-N or hPLEIADf: ex4term, was sufficient for the interaction (3D and 4D), while the C-terminal region, hPLEIAD-C, shared by both hPLEIADa and f, failed to undergo detectable interaction (5D). Two different mutations in PXDLS-binding domain of CTB1 showed negative effect on its interaction with PLEIAD (2F to 4F and 2H to 4H). (c) Complex formation of CAPN3, PLEIAD, and CTBP1 was examined using wheat-germ cell-free expression system. In addition to the layer of mRNA and other components for translation reaction, solution of CTBP1 protein was set on the bottom of the tube. After translation, layers were mixed and subjected to immunoprecipitation using anti-CAPN3 antibody. (d) Both PLEIADa and PLEIADf were coimmunoprecipitated with CAPN3:CS (lanes 5 and 7, CBB and anti-His). In these samples, CTBP1 was also detected (anti-CTBP1). Numbers in parentheses indicate the percentage of the total amount. Nonspecific degradation or precipitation of CTBP1 during translation reaction was not detected (data not shown).

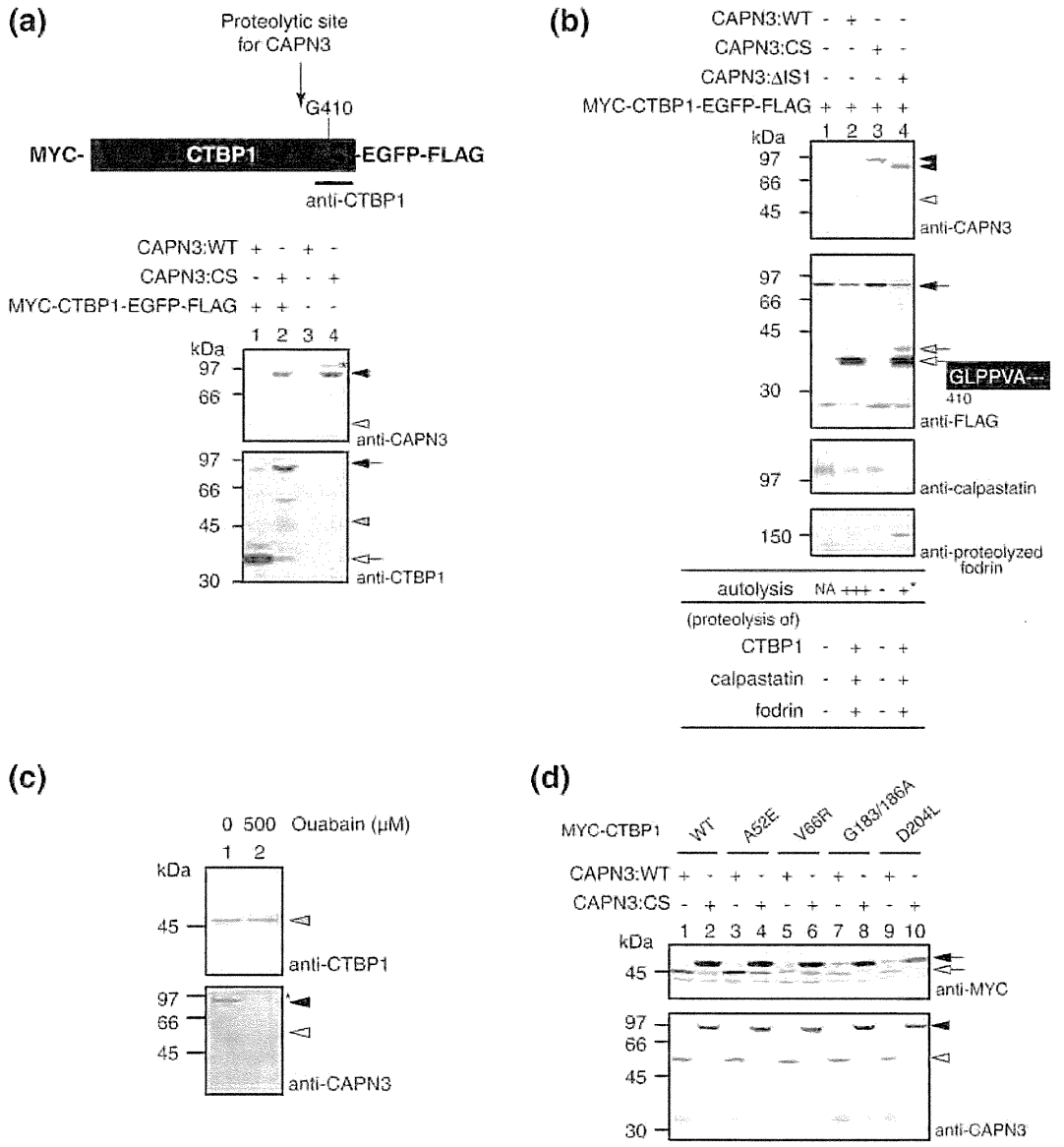


**Fig. 4.** CTBP1, a binding protein for PLEIAD, is a potential CAPN3 substrate. (a) Triple-tagged CTBP1 (MYC-CTBP1-EGFP-FLAG) expressed in COS7 cells was proteolyzed when CAPN3:WT was coexpressed (lane 1). This CTBP1 construct was susceptible to proteolysis (lane 2), but the difference between lanes 1 and 2 was still significant. In the cells expressing CAPN3:WT, the endogenous CTBP1 was undetectable (compare lanes 3 and 4). (b) Proteolysis of the CTBP1 construct was also observed in COS7 cells coexpressing mouse CAPN3:ΔIS1 (lane 4, anti-FLAG); CAPN3:ΔIS1 is a splicing variant that shows protease activity comparable to that of WT but lacks the autolytic sites encoded by exon 6. The C-terminal proteolyzed fragment of the CTBP1 construct was immunoprecipitated by anti-FLAG, and its N-terminal sequence was determined. (c) In cultured myotubes, the activation of CAPN3 by ouabain treatment did not cause significant proteolysis of endogenous CTBP1 protein (lane 2). (d) Proteolysis of CTBP1 by CAPN3 depends on functional structure of CTBP1. Four different CTBP1 mutants (see Fig. 3a) were coexpressed with CAPN3:WT or CAPN3:CS. In contrast to wild-type CTBP1, three of the mutants showed altered susceptibility to proteolysis (lanes 5, 7, and 9). For the mutant A52E, no significant change was observed (lane 3). Closed and open arrowheads indicate the full-length and autolytic fragments of CAPN3, respectively, detected by Western blotting using an anti-CAPN3 antibody. Gray arrowheads indicate endogenous CTBP1. Closed, open, and gray arrows indicate the full-length, the main, and the minor proteolyzed fragment of the CTBP1 construct expressed in COS7 cells, respectively.

different subcellular compartments, we sought to identify molecular interactions that affect its protease activity. Here, we showed that PLEIAD/SIMC1/C5orf25, a novel CAPN3-binding protein, moderates the protease activity of CAPN3 and possesses the potential to function as a scaffold protein.

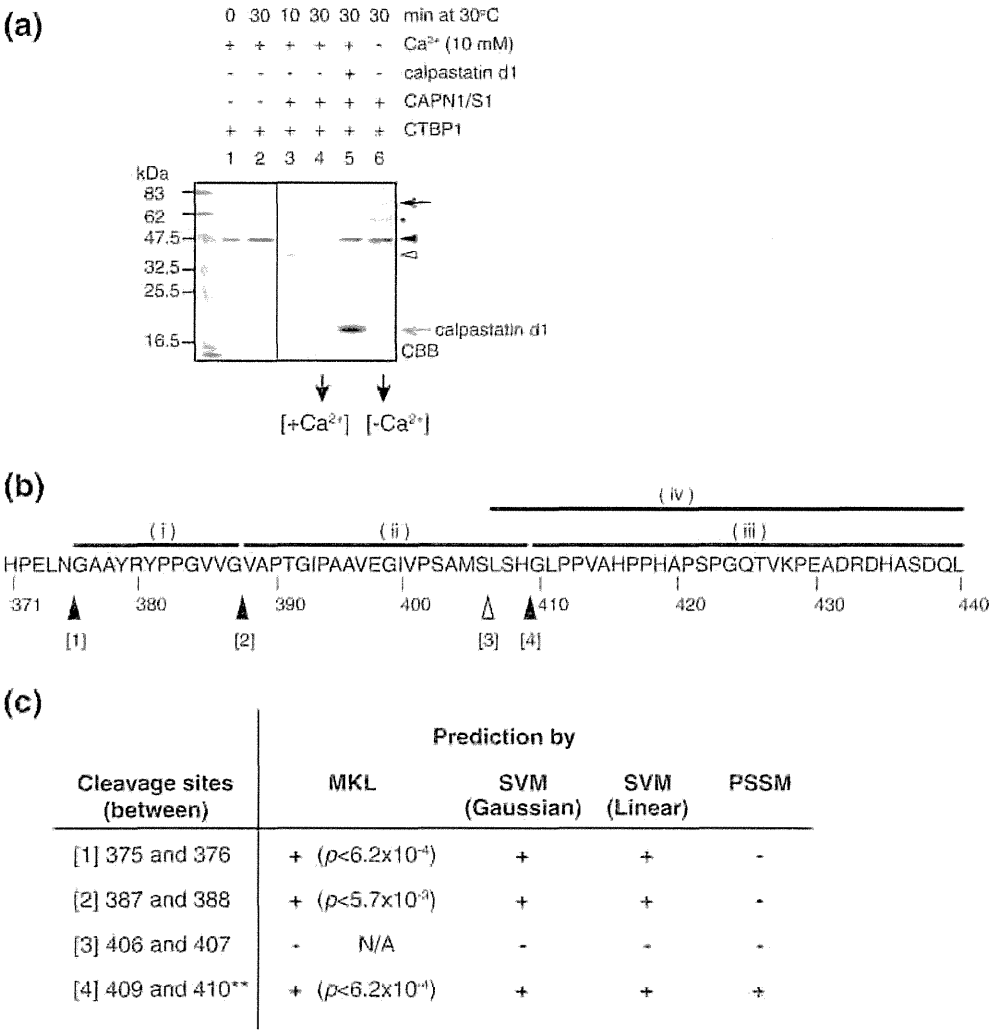


**Fig. 5.** Proteolysis of CTBP1 by classical calpain, μ-calpain (CAPN1/S1), revealed additional cleavage sites. (a) Recombinant CTBP1 protein was incubated under the conditions indicated at the top. CTBP1 was proteolyzed by CAPN1/S1 in the presence of $Ca^{2+}$ (lane 4), and this reaction was inhibited by calpastatin peptide (lane 5). Peptide fractions generated in the presence (lane 4, [+$Ca^{2+}$]) or in the absence (lane 6, [−$Ca^{2+}$]) of $Ca^{2+}$ were further analyzed by mass spectrometry. Closed and open arrowheads indicate the full-length and the main proteolyzed fragment of recombinant CTBP1. Closed and open arrows indicate CAPN1 and recombinant calpastatin domain 1. *, unidentified signal. (b) Four peptides were identified in the [+$Ca^{2+}$] sample [horizontal bars (i) to (iv)], and four cleavage sites by CAPN1/S1 at the C-terminus of CTBP1 were revealed (vertical arrowheads, [1] to [4]). Two sequences, (iii) and (iv), were also detected in the [−$Ca^{2+}$] sample, suggesting that the peptide bonds at positions [3] and [4] have a propensity to be hydrolyzed. (c) Calpain cleavage sites in CTBP1 were predicted using our predictor available at http://www.calpain.org. Three cleavage sites, [1], [2], and [4], coincided with those predicted by at least three different algorithms. +, predicted; −, not predicted; **, biochemically identified as the cleavage site for CAPN3 [Fig. 4, (c)].

## PLEIAD is a novel CAPN3-regulating protein

So far, this is the first report on the functional properties of PLEIAD. In addition, we have shown that, in skm, a *Pleiad* transcript that lacks exons 2 and 3 is the predominant variant. Notably, this PLEIAD variant has not been identified in other human tissues, such as brain or testis, strongly suggesting that it is a low-abundance isoform that may be muscle specific. Unlike CAPN3, the ubiquitous expression of PLEIAD has been shown in databases at both transcript[†] and protein levels.[‡] The differential expression of PLEIAD has been detected by the transcriptional profiling of many diseases, including muscular dystrophies,[38] but it is not clear if these changes are related to CAPN3's functions. YTH screening revealed that PLEIAD also interacts with CTBP1, and it may interact with other cytosolic and/or cytoskeletal proteins. Therefore, further studies are necessary to address the

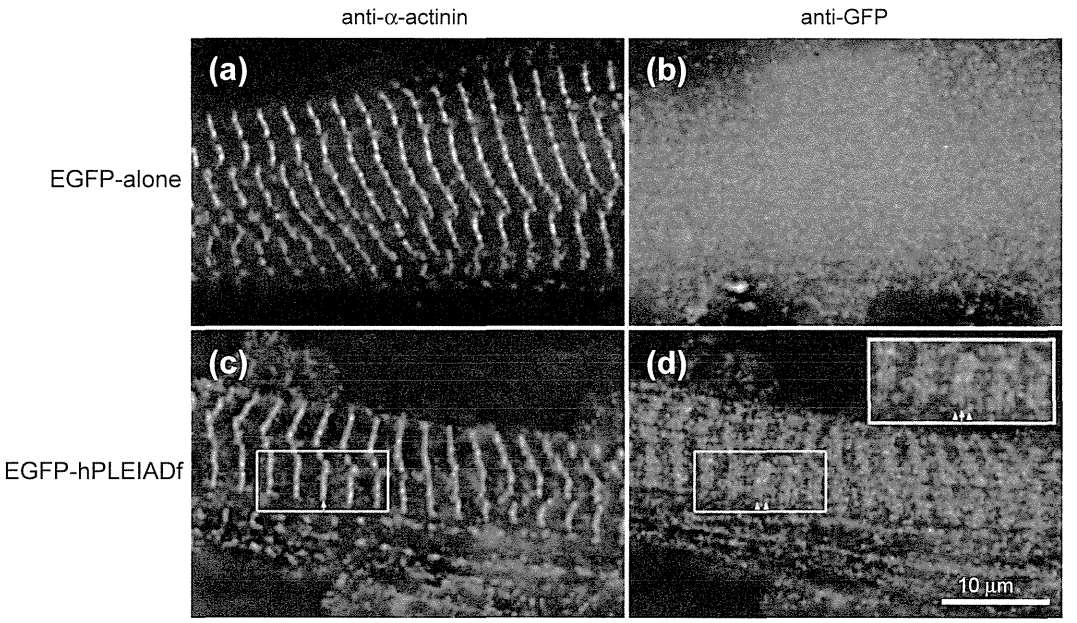


**Fig. 6.** PLEIAD shows diffuse cytoplasmic localization in skeletal myotubes. Localization of expressed EGFP-hPLEIADf was examined in cultured chick skeletal myotubes. Cells were stained with anti-sarcomeric α-actinin (a and d) and anti-GFP antibodies (b and d). The primary localization of hPLEIADf was diffusely cytoplasmic (data not shown). Occasionally, in about 10% of transfected cells, EGFP-hPLEIADf was localized in a striated pattern within the sarcomeric I band, on each side of the Z-line (d, inset). Arrow and arrowheads indicate a Z-line labeled by α-actinin and EGFP-hPLEIADf, respectively. The scale bar represents 10 μm.

possibility that PLEIAD has many functional links to other proteins, not only in skm but also in other tissues. The two recently identified tandem SUMO-interacting motifs at PLEIAD's N-terminus also indicate its potential roles in signaling pathways regulated by sumoylation. Another interesting finding is that humans have one PLEIAD pseudogene (*PLEIAD-ps1*, originally called *LOC202181*) close to *PLEIAD* (5q35.3 and 5q35.2, respectively).

From the viewpoint of molecular evolution, it is noteworthy that the C-terminal region of PLEIAD, which is responsible for the CAPN3 suppressor effect, is significantly conserved from human to fish and that CAPN3 is also evolutionarily conserved among vertebrates. There are, however, some inconsistencies: (1) The mouse ortholog, mPLEIAD, is much larger than the orthologs found in most mammals. The observed increase in protein size is caused by the insertion of a highly repetitive sequence in mouse exon 2, which corresponds to human exon 4. (2) At least in human and in mouse, one splicing variant has a structurally identical exon composition, and this variant lacks exon 4 in the human and exon 2 in the mouse [Figs. 1b, (c:Δex2-4) and 2c, (b)], respectively. Although these variants were not detected in skm in our hands, the identified transcripts in lower vertebrates show more similarity to these variants and lack the N-terminal region. (3) The ortholog found in marsupials, *Monodelphis domestica* (opossum), lacks the sequence corresponding to the Pro-rich region in hPLEIAD [Fig. 2a, (4)].[39] It is a serious concern that potential sequencing errors in databases could result in our misinterpretation of the structure of PLEIAD homologs, while our sequence analyses suggested that the PLEIAD gene has been a target of evolutionary modification by repetitive sequences, such as transposable elements.[40] These findings complicate our conclusion regarding the canonical functional structure of PLEIAD. In particular, the second point described above argues against the simple explanation that the N-terminal region of PLEIAD recruits substrates while its C-terminal region suppresses the CAPN3 protease activity. It is possible that the CAPN3-suppressing activity was conserved during vertebrate evolution, whereas the functions of the N-terminal parts diverged. It is nonetheless tempting to speculate that the N-terminal substrate scaffold function is applicable to the PLEIAD orthologs found in large mammals such as human and bovines.

### Relevance of the C-terminal cleavage in CTBP1 functions

Our biochemical evidence indicated that CTBP1 is a good substrate for calpains including CAPN3. CTBP1 has multiple functions in both the nucleus and the cytoplasm.[30,31,41,42] In particular, its function

as a nuclear transcriptional regulator has been well studied.[43–45] CTBP1's regulation is important for proper proliferation and differentiation.[45–49] For example, the down-regulation of CTBP1 at the protein level, which is catalyzed by the ubiquitin-proteasome pathway,[50] counteracts oncogenic gene expression.[51] In addition, phosphorylation and sumoylation at the C-terminus of CTBP1 exert regulatory effects.[42] Notably, CTBP1's cleavage by calpains removes these modification sites, suggesting that calpains also participate in the regulation of CTBP1, although we could not detect this cleavage *in vivo*.

The function of CTBP1 in skm remains unclear; therefore, it is difficult to speculate about what the outcomes of CAPN3-mediated CTBP1 proteolysis are. One possibility is that the regulation of CTBP1 by CAPN3 is functionally analogous to a previously proposed role of CAPN3 in down-regulating β-catenin in skm.[13] Since CTBP1 itself is capable of carrying out multi-directional functions, its stage-specific regulation may be involved in skm cell fusion and development into myotubes.

For the interaction between CTBP1 and PLEIAD, it was suggested that PXDLS-binding site on CTBP1 is involved at the level of YTH assay, and further analyses are required to evaluate its biological significance. It was also suggested that CAPN3 recognizes the structure of CTBP1 relevant for its PXDLS binding and NAD(H) binding. However, there is a possibility that the selected CTBP1 mutations have too strong effect on the overall structure of the molecule and the essential structure of CTBP1 as a substrate for calpain warrants further investigation.

### Possible link between the CAPN3–PLEIAD and CAPN3–connectin/titin interactions

We previously proposed that the N2A region of connectin/titin supports the functions of CAPN3 by stabilizing CAPN3 while it recruits MARPs (*m*uscle *a*nkyrin *r*epeat *p*roteins) as substrates for CAPN3. Such a model is physically possible for connectin/titin, since it is located in sarcomeres, which are mostly composed of extension-competent structures, such as immunoglobulin motifs and fibronectin type III-like domains. From the primary sequence of PLEIAD, it is not clear if a robust structural change occurs upon its interaction with CAPN3 and/or CTBP1. Still, it is worth noting that the C-terminal functional region of PLEIAD has no defined structure and/or motif. The specificity and efficiency of calpastatin, a specific inhibitory protein for classical calpains except CAPN3, relies on its unstructured nature; it is classified as an intrinsically unstructured/disordered protein[52]; calpastatin binds close to, but loops out into, the side opposite calpain's active site, escaping cleavage by the calpain.[53,54] Although there is not a strong sequence similarity between PLEIAD and calpastatin, it is possible that PLEIAD functions in an analogous manner. We also hypothesize that the N-terminal region of PLEIAD is involved in the regulation of CAPN3 autolysis by increasing the affinity of the molecule to the full-length, pre-autolyzed form of CAPN3 but is susceptible to protease activity of CAPN3. On the other hand, the C-terminal region of PLEIAD is resistant to protease activity of CAPN3 but has lower ability to interact with CAPN3 by its own.

We sought to detect endogenous mPLEIAD in mouse tissues using two commercially available anti-hPLEIAD antibodies. These antibodies did not yield consistent results; thus, we suspended our analysis of mouse PLEIAD localization during the preparation of this manuscript. Instead, we used an alternative approach, the expression of hPLEIAD in chicken primary cultured skeletal myotubes. The localization of expressed hPLEIADf (see Fig. 6) showed that this new regulator of CAPN3 is primarily distributed diffusely in the cytoplasm. At the same time, the occasional localization of hPLEIADf within the sarcomeric I-band region raises the intriguing possibility that connectin/titin and PLEIAD cooperate as CAPN3 regulators. Further investigation of the spatiotemporal expression of the PLEIAD protein in skm is required in order to address this issue.

In this study, a novel protein–protein interaction that is capable of regulating CAPN3 in the cytoplasm as well as in the sarcomere was shown. Along with the identification of possible CAPN3 functions in different cellular compartments, it has been unknown how CAPN3 avoids autolytic degradation while it is translocated. We anticipate that the present study will serve as a good starting point toward understanding how CAPN3 conducts its multiple functions. It is likely that there are other interacting molecules relevant to CAPN3's functions that are yet to be discovered.

## Materials and Methods

### Experimental animals

All procedures used for experimental animals were approved by the Experimental Animal Care and Use Committee of Tokyo Metropolitan Institute of Medical Science, and the animals and related materials were treated in accordance with the committee's guidelines.

### cDNA constructs

The cDNA clone for PLEIAD/C5orf25, which was originally purchased from Ressourcenzentrum Primärdatenbank (German Science Centre for Genome Research), is now available from Source BioScience (IRATp970H0629D). The cDNAs for human CAPN3 and mouse CAPN3Δ1 were subcloned into the pSRD expression vector for

protein expression in mammalian cells, as described previously.[25,35] These cDNAs were also expressed as N-terminal FLAG-tagged or MYC-tagged proteins using the pSRD or pcDNA3.1 expression vector (Invitrogen, Grand Island, NY).[55] The pEGFP-C1 expression vector was also used. For the YTH assay, the pAS2-1c[25] and pACT2 expression vectors (U29899; Clontech, Mountain View, CA) were used. Enzymes used to manipulate recombinant DNA were purchased from Takara Bio (Shiga, Japan) or New England Biolabs (Ipswich, MA). The mutations described here were introduced by long PCR using *Pfu*-Turbo DNA polymerase, as described previously.[56] All the constructs were verified by DNA sequencing.

### PCR and RT-PCR analyses

Endpoint PCR reactions to detect the expression of C5orf25 were performed using ExTaq DNA polymerase (Takara) and the appropriate primer pairs (Fig. 1b and Table 1). Some PCR products were sequenced for verification. The human skm cDNA library for YTH (Clontech) or mouse skm cDNA synthesized from total RNA was used as a template. Total RNA was prepared from cultured mouse muscle cells and the quadriceps femoris of 30-week-old C57BL/6J mice using TRIzol® Reagent (Invitrogen), according to the manufacturer's instructions. For RT by PrimeScript® Reverse Transcriptase (Takara), 1.5 μg and 1.1 μg of total RNA from cultured cells and tissues, respectively, were used per 10-μl reaction.

### Cell culture and protein expression

Protein expression in HEK293 cells was performed as previously described.[28] COS7 cells were grown in Dulbecco's modified Eagle's medium (Sigma-Aldrich, St. Louis, MO) supplemented with 10% fetal bovine serum that had been heat inactivated at 56 °C for 30 min before use. For recombinant protein expression in COS7 cells, the plasmid was prepared at a concentration of 1 μg/μl and transfected using TransIT®-LT1 (Mirus Bio LLC, Madison, WI). As a standard, 2–4 μg of plasmid plus a 3× volume of transfection reagent were used per $1.5 \times 10^5$ cells plated in 3.5-cm dish, 12–16 h prior to transfection. The cells were harvested 40–60 h after transfection using ice-cold phosphate-buffered saline.[26]

Primary cultures of chick skeletal myotubes were prepared as described previously.[57] Cells used for immunofluorescence were grown on coverslips coated with Matrigel™ (BD Biosciences, San Jose, CA) diluted to 0.5 mg/ml in minimum essential medium. Transfection was performed 12–16 h after plating using Effectene (Qiagen, Valencia, CA), as previously described.[58] Primary cultures of mouse skm cells were prepared as described previously.[27] Cells were allowed to differentiate for 5 and 10 days and used for total RNA purification and a 2-h incubation with ouabain, respectively.

*In vitro* transcription and translation were performed using a wheat-germ cell-free expression system, according to the manufacturer's instructions (CellFree Sciences, Japan). The mRNAs for each construct were transcribed separately. The translation reaction was carried out at 16 °C for 18–20 h without shaking. Two micrograms of recombinant CTBP1 (1 mg/ml stock solution) was added to the bottom of 112-μl translation reaction mixture.

### Immunoprecipitation

Harvested cells were suspended in lysis buffer [50 mM Tris–HCl (pH 7.5), 150 mM CsCl, 1 mM ethylenediaminetetraacetic acid-KOH (pH 8.0), and 1% Triton X-100] containing protease inhibitors [1 mM 4-(2-aminoethyl) benzenesulfonyl fluoride hydrochloride, 0.1 mM leupeptin, 10 μg/ml aprotinin, and 10 mM iodoacetamide] and incubated on ice for 30 min with occasional mixing. The supernatant was collected after centrifugation at 20,630***g*** at 4 °C for 15 min. Incubation with anti-FLAG M2 affinity gel (Sigma-Aldrich) and elution of the immunoprecipitated proteins were performed according to the manufacturer's instructions using a modified wash buffer [50 mM Tris–HCl (pH 7.5) and 150 mM CsCl].[26] To detect the CAPN3–PLEIAD interaction, we carried out the incubation for 2–3 h. When anti-CAPN3 antibody was used for immunoprecipitation, the immunocomplex was recovered by Protein-G Sepharose (GE Healthcare). The eluate was subjected to SDS-PAGE and Western blot analysis. For N-terminal sequencing, the immunoprecipitated proteins were blotted onto a ProBlott membrane (Applied Biosystems, Carlsbad, CA) after SDS-PAGE. The target protein bands were visualized by CBB G-250 staining, excised, and submitted to APRO Science Institute Inc. (Tokushima, Japan) for sequence analysis.

### Western blot analysis

Proteins were separated by SDS-PAGE and transferred onto polyvinylidene fluoride membranes (Millipore, Bedford, MA). The membranes were probed with the appropriate primary antibodies and horseradish-peroxidase-coupled secondary antibodies (Nichirei, Tokyo, Japan) followed by visualization using a POD immunostaining kit (Wako, Osaka, Japan) or SuperSignal® West Pico Chemiluminescent Substrate (Pierce, Rockford, IL).[26] Scanned images were processed for presentation using Adobe Photoshop CS6 (Adobe Systems, San Jose, CA).

### Immunofluorescence analysis

Immunofluorescence microscopy was performed as described previously.[58] At 4–5 days after transfection, the cells were incubated in relaxing buffer [150 mM KCl, 5 mM $MgCl_2$, 10 mM 3-(*N*-morpholino) propanesulfonic acid (pH 7.4), 1 mM ethylene glycol bis(β-aminoethyl ether) *N,N'*-tetraacetic acid, and 4 mM ATP] for 15 min, followed by fixation using 2% formaldehyde in relaxing buffer for 15 min. The primary and secondary antibodies were used at the concentrations described in Antibodies. Coverslips were mounted onto slides with Aqua Poly/Mount (Polysciences, Warrington, PA), and the samples were analyzed on an Axiovert microscope (Zeiss, Oberkochen, Germany) using 63× (NA 1.4) or 100× (NA 1.3) objectives. The cells were also analyzed using a Deltavision RT system (Applied Precision, Issaquah, WA) with an inverted microscope (IS70; Olympus, Tokyo, Japan), a

100× (NA 1.3) objective, and a charge-coupled device camera (CoolSNAP HQ; Photometrics, Huntington Beach, CA). The images were deconvolved using SoftWoRx 3.5.1 software (Applied Precision) and processed for presentation using Adobe Photoshop CS6 (Adobe Systems).

### Antibodies

The antibodies used in this study include anti-FLAG mouse monoclonal (1:1000, M2; Stratagene, La Jolla, CA), anti-MYC mouse monoclonal (1:1000, 9E10; Developmental Studies Hybridoma Bank), anti-calpastatin mouse monoclonal (1:1000, PI-11; American Type Culture Collection), anti-CTBP1 mouse monoclonal (1:1000, 3/CtBP1; BD Transduction Laboratories™), anti-α-actinin mouse monoclonal (1:2000, EA-53; Sigma-Aldrich), anti-GFP rabbit polyclonal (1:2000; Abcam, Cambridge, MA), anti-CAPN3 goat polyclonal (1:1000; Cosmo Bio, Tokyo, Japan), anti-His mouse monoclonal (1:2000; Novagen), and anti-proteolyzed fodrin (anti-GMMPR) rabbit polyclonal (1:1000, anti-GMMPR) antibodies.[26,32] As secondary antibodies, Alexa Fluor 488-conjugated goat anti-rabbit IgG (1:1000; Invitrogen) and Texas Red-conjugated donkey anti-mouse IgG (1:600; Jackson Immunoresearch Laboratories, West Grove, PA) antibodies were used.

### Protein identification by mass spectrometry

The FLAG-immunoprecipitates from HEK293 cells were analyzed using direct nanoflow liquid chromatography coupled with tandem mass spectrometry.[28] To identify the peptide sequence generated during the *in vitro* proteolysis of CTBP1, we desalted the reaction solution using ZipTip® Pipette Tips (Millipore), and tandem mass spectrometry spectra were acquired by a 4800 MALDI TOF/TOF™ analyzer (AB SCIEX, Framingham, MA). Data were analyzed by Protein Pilot™ software (version 4.5) (AB SCIEX).

### Calpain cleavage assay *in vitro*

Two hundred nanograms of recombinant human CTBP1 (ProSpec, Ness Ziona, Israel) was incubated with 25 ng of recombinant human CAPN1/S1 (μ-calpain) (BioVision, Milpitas, CA) in 10 μl of incubation buffer [20 mM Tris–HCl (pH 8.0), 1 mM ethylenediaminetetraacetic acid-KOH (pH 8.0), and 1 mM DTT] with or without 10 mM $CaCl_2$ at 30 °C for 10 and 30 min. Where indicated, recombinant human calpastatin domain I (Takara) was added to a concentration of 29 mM. The reaction was stopped by the addition of SDS sample buffer, and the sample was subjected to SDS-PAGE followed by CBB G-250 staining.

### YTH assay

Proteins interacting with C5orf25 were screened as previously reported[22] using *Saccharomyces cerevisiae* strain AH109. The full-length PLEIAD cDNA cloned into pAS2-1c was coexpressed in the yeast with approximately $1.3 \times 10^6$ of a human skm cDNA library in the pGAD424 vector (Clontech). The plasmids were rescued from colonies grown on SD medium that lacked Leu, Trp, His, and Ade (SD-LWHA) and were sequenced. The rescued plasmids were retransformed with a series of PLEIAD mutants using the Fast™-Yeast Transformation Kit (G-Biosciences/Genotech, St. Louis, MO), according to the manufacturer's instructions. Cotransformants were selected on SD-LW plates, and the expressions of reporter genes were assessed by growth on SD-LWHA plates.

### Sequence analysis

Sequence data were retrieved from the NCBI[§] and Ensembl[‖] databases. The sequences from UniProtKB[¶] were also used to check the consistency. BLAST searches were performed with psi-BLAST and BLAST-p and tBLAST-n *versus* the nonredundant protein or nucleotide databases. For phylogenetic analysis, sequences were aligned using MAFFT[a59] and converted to an unrooted tree diagram after manual inspection. The identity and similarity of aligned sequences were calculated using Genetyx (version 11) (Genetyx Co., Tokyo, Japan). Sequence repeats were identified with RADAR,[b60] and designated sequences were aligned using MAFFT and Genetyx. To predict calpain cleavage sites, we analyzed the protein sequences with an online cleavage site predictor.[c7,36,61]

## Acknowledgements

We thank all the Calpain Project laboratory members for their invaluable support. This work was supported in part by Japan Society for the Promotion of Science Grants-in-Aid for Scientific Research, 20370055 and 23247021 (to H.S.) and 22770139 (to Y.O.); a Takeda Science Foundation research grant (to H.S.); the Collaborative Research Program of the Institute for Chemical Research; Kyoto University, grant 2010-15 (to H.S.) and grants 2011-18 and 2012-30 (to Y.O.); Toray Science and Technology Grant (to Y.O.); American Heart Association Pre-Doctoral Fellowship 12PRE11900038 (to S.M.N.); and National Institutes of Health Grants HL083146 and HL108625 (to C.C.G.).

*Received 30 January 2013;*
*Received in revised form 28 April 2013;*
*Accepted 15 May 2013*
Available online 21 May 2013

***Keywords:***
calpain;
skeletal muscle;
autolysis;
scaffold;
substrate

Present address: S. Iemura, Innovative Drug Development Translational Research Section, Fukushima Medical University, 1 Hikariga-oka, Fukushima City, Fukushima Prefecture 960-1295, Japan.

†For example, see http://www.ebi.ac.uk/gxa/gene/ENSG00000170085.
‡For example, see http://www.ebi.ac.uk/pride/searchSummary.do?queryTypeSelected=identification%20accession%20number&identificationAccessionNumber=Q8NDZ2.
§http://www.ncbi.nlm.nih.gov/
‖http://ensembl.org/
¶http://www.uniprot.org/
[a]http://www.genome.jp/tools/mafft/
[b]http://www.ebi.ac.uk/Tools/pfa/
[c]http://calpain.org/

***Abbreviations used:***
NCBI, National Center for Biotechnology Information; YTH, yeast two-hybrid.

## References

1. Sorimachi, H., Imajoh-Ohmi, S., Emori, Y., Kawasaki, H., Ohno, S., Minami, Y. & Suzuki, K. (1989). Molecular cloning of a novel mammalian calcium-dependent protease distinct from both m- and mu-types. Specific expression of the mRNA in skeletal muscle. *J. Biol. Chem.* **264**, 20106–20111.
2. Goll, D. E., Thompson, V. F., Li, H., Wei, W. & Cong, J. (2003). The calpain system. *Physiol. Rev.* **83**, 731–801.
3. Liu, J., Liu, M. C. & Wang, K. K. (2008). Calpain in the CNS: from synaptic function to neurotoxicity. *Sci. Signaling*, **1**, re1.
4. Sorimachi, H., Hata, S. & Ono, Y. (2011). Calpain chronicle—an enzyme family under multidisciplinary characterization. *Proc. Jpn. Acad., Ser. B*, **87**, 287–327.
5. Sorimachi, H., Hata, S. & Ono, Y. (2011). Impact of genetic insights into calpain biology. *J. Biochem.* **150**, 23–37.
6. Ono, Y. & Sorimachi, H. (2012). Calpains: an elaborate proteolytic system. *Biochim. Biophys. Acta*, **1824**, 224–236.
7. Sorimachi, H., Mamitsuka, H. & Ono, Y. (2012). Understanding the substrate specificity of conventional calpains. *Biol. Chem.* **393**, 853–871.
8. Richard, I., Broux, O., Allamand, V., Fougerousse, F., Chiannilkulchai, N., Bourg, N. *et al.* (1995). Mutations in the proteolytic enzyme calpain 3 cause limb-girdle muscular dystrophy type 2A. *Cell*, **81**, 27–40.
9. Beckmann, J. S. & Spencer, M. (2008). Calpain 3, the "gatekeeper" of proper sarcomere assembly, turnover and maintenance. *Neuromuscular Disord.* **18**, 913–921.
10. Richard, I., Roudaut, C., Marchand, S., Baghdiguian, S., Herasse, M., Stockholm, D. *et al.* (2000). Loss of calpain 3 proteolytic activity leads to muscular dystrophy and to apoptosis-associated IκBα/nuclear factor κB pathway perturbation in mice. *J. Cell Biol.* **151**, 1583–1590.
11. Fougerousse, F., Gonin, P., Durand, M., Richard, I. & Raymackers, J. M. (2003). Force impairment in calpain 3-deficient mice is not correlated with mechanical disruption. *Muscle Nerve*, **27**, 616–623.
12. Kramerova, I., Kudryashova, E., Tidball, J. G. & Spencer, M. J. (2004). Null mutation of calpain 3 (p94) in mice causes abnormal sarcomere formation *in vivo* and *in vitro*. *Hum. Mol. Genet.* **13**, 1373–1388.
13. Kramerova, I., Kudryashova, E., Wu, B. & Spencer, M. J. (2006). Regulation of the M-cadherin-β-catenin complex by calpain 3 during terminal stages of myogenic differentiation. *Mol. Cell. Biol.* **26**, 8437–8447.
14. Kramerova, I., Kudryashova, E., Wu, B., Ottenheijm, C., Granzier, H. & Spencer, M. J. (2008). Novel role of calpain-3 in the triad-associated protein complex regulating calcium release in skeletal muscle. *Hum. Mol. Genet.* **17**, 3271–3280.
15. Kramerova, I., Kudryashova, E., Wu, B., Germain, S., Vandenborne, K., Romain, N. *et al.* (2009). Mitochondrial abnormalities, energy deficit and oxidative stress are features of calpain 3 deficiency in skeletal muscle. *Hum. Mol. Genet.* **18**, 3194–3205.
16. Kramerova, I., Kudryashova, E., Ermolova, N., Saenz, A., Jaka, O., Lopez de Munain, A. & Spencer, M. J. (2012). Impaired calcium calmodulin kinase signaling and muscle adaptation response in the absence of calpain 3. *Hum. Mol. Genet.* **21**, 3193–3204.
17. Jaka, O., Kramerova, I., Azpitarte, M., Lopez de Munain, A., Spencer, M. & Saenz, A. (2012). C3KO mouse expression analysis: downregulation of the muscular dystrophy Ky protein and alterations in muscle aging. *Neurogenetics*, **13**, 347–357.
18. Ojima, K., Kawabata, Y., Nakao, H., Nakao, K., Doi, N., Kitamura, F. *et al.* (2010). Dynamic distribution of muscle-specific calpain in mice has a key role in physical-stress adaptation and is impaired in muscular dystrophy. *J. Clin. Invest.* **120**, 2672–2683.
19. Ojima, K., Ono, Y., Ottenheijm, C., Hata, S., Suzuki, H., Granzier, H. & Sorimachi, H. (2011). Non-proteolytic functions of calpain-3 in sarcoplasmic reticulum in skeletal muscles. *J. Mol. Biol.* **407**, 439–449.
20. Tagawa, K., Taya, C., Hayashi, Y., Nakagawa, M., Ono, Y., Fukuda, R. *et al.* (2000). Myopathy phenotype of transgenic mice expressing active site-mutated inactive p94 skeletal muscle-specific calpain, the gene product responsible for limb girdle muscular dystrophy type 2A. *Hum. Mol. Genet.* **9**, 1393–1402.
21. Sorimachi, H., Toyama-Sorimachi, N., Saido, T. C., Kawasaki, H., Sugita, H., Miyasaka, M. *et al.* (1993). Muscle-specific calpain, p94, is degraded by autolysis immediately after translation, resulting in disappearance from muscle. *J. Biol. Chem.* **268**, 10593–10605.
22. Sorimachi, H., Kinbara, K., Kimura, S., Takahashi, M., Ishiura, S., Sasagawa, N. *et al.* (1995). Muscle-specific calpain, p94, responsible for limb girdle muscular dystrophy type 2A, associates with connectin through IS2, a p94-specific sequence. *J. Biol. Chem.* **270**, 31158–31162.

23. Kinbara, K., Sorimachi, H., Ishiura, S. & Suzuki, K. (1997). Muscle-specific calpain, p94, interacts with the extreme C-terminal region of connectin, a unique region flanked by two immunoglobulin C2 motifs. *Arch. Biochem. Biophys.* **342**, 99–107.
24. Kinbara, K., Ishiura, S., Tomioka, S., Sorimachi, H., Jeong, S. Y., Amano, S. *et al.* (1998). Purification of native p94, a muscle-specific calpain, and characterization of its autolysis. *Biochem. J.* **335**, 589–596.
25. Ono, Y., Torii, F., Ojima, K., Doi, N., Yoshioka, K., Kawabata, Y. *et al.* (2006). Suppressed disassembly of autolyzing p94/CAPN3 by N2A connectin/titin in a genetic reporter system. *J. Biol. Chem.* **281**, 18519–18531.
26. Hayashi, C., Ono, Y., Doi, N., Kitamura, F., Tagami, M., Mineki, R. *et al.* (2008). Multiple molecular interactions implicate the connectin/titin N2A region as a modulating scaffold for p94/calpain 3 activity in skeletal muscle. *J. Biol. Chem.* **283**, 14801–14814.
27. Ojima, K., Ono, Y., Doi, N., Yoshioka, K., Kawabata, Y., Labeit, S. & Sorimachi, H. (2007). Myogenic stage, sarcomere length, and protease activity modulate localization of muscle-specific calpain. *J. Biol. Chem.* **282**, 14493–14504.
28. Natsume, T., Yamauchi, Y., Nakayama, H., Shinkawa, T., Yanagida, M., Takahashi, N. & Isobe, T. (2002). A direct nanoflow liquid chromatography-tandem mass spectrometry system for interaction proteomics. *Anal. Chem.* **74**, 4725–4733.
29. Sun, H. & Hunter, T. (2012). Poly-small ubiquitin-like modifier (PolySUMO)-binding proteins identified through a string search. *J. Biol. Chem.* **287**, 42071–42083.
30. Corda, D., Colanzi, A. & Luini, A. (2006). The multiple activities of CtBP/BARS proteins: the Golgi view. *Trends Cell Biol.* **16**, 167–173.
31. Chinnadurai, G. (2009). The transcriptional corepressor CtBP: a foe of multiple tumor suppressors. *Cancer Res.* **69**, 731–734.
32. Ono, Y., Ojima, K., Torii, F., Takaya, E., Doi, N., Nakagawa, K. *et al.* (2010). Skeletal muscle-specific calpain is an intracellular $Na^+$-dependent protease. *J. Biol. Chem.* **285**, 22986–22998.
33. Matsuoka, S., Ballif, B. A., Smogorzewska, A., McDonald, E. R., 3rd, Hurov, K. E., Luo, J. *et al.* (2007). ATM and ATR substrate analysis reveals extensive protein networks responsive to DNA damage. *Science*, **316**, 1160–1166.
34. Kuppuswamy, M., Vijayalingam, S., Zhao, L. J., Zhou, Y., Subramanian, T., Ryerse, J. & Chinnadurai, G. (2008). Role of the PLDLS-binding cleft region of CtBP1 in recruitment of core and auxiliary components of the corepressor complex. *Mol. Cell. Biol.* **28**, 269–281.
35. Herasse, M., Ono, Y., Fougerousse, F., Kimura, E., Stockholm, D., Beley, C. *et al.* (1999). Expression and functional characteristics of calpain 3 isoforms generated through tissue-specific transcriptional and posttranscriptional events. *Mol. Cell. Biol.* **19**, 4047–4055.
36. duVerle, D. A., Ono, Y., Sorimachi, H. & Mamitsuka, H. (2011). Calpain cleavage prediction using multiple kernel learning. *PLoS One*, **6**, e19035.
37. Ma, H., Shih, M., Fukiage, C., Azuma, M., Duncan, M. K., Reed, N. A. *et al.* (2000). Influence of specific regions in Lp82 calpain on protein stability, activity, and localization within lens. *Invest. Ophthalmol. Visual Sci.* **41**, 4232–4239.
38. Bakay, M., Wang, Z., Melcon, G., Schiltz, L., Xuan, J., Zhao, P. *et al.* (2006). Nuclear envelope dystrophies show a transcriptional fingerprint suggesting disruption of Rb-MyoD pathways in muscle regeneration. *Brain*, **129**, 996–1013.
39. Mikkelsen, T. S., Wakefield, M. J., Aken, B., Amemiya, C. T., Chang, J. L., Duke, S. *et al.* (2007). Genome of the marsupial *Monodelphis domestica* reveals innovation in non-coding sequences. *Nature*, **447**, 167–177.
40. Jurka, J., Kapitonov, V. V., Kohany, O. & Jurka, M. V. (2007). Repetitive sequences in complex genomes: structure and evolution. *Annu. Rev. Genomics Hum. Genet.* **8**, 241–259.
41. Riefler, G. M. & Firestein, B. L. (2001). Binding of neuronal nitric-oxide synthase (nNOS) to carboxyl-terminal-binding protein (CtBP) changes the localization of CtBP from the nucleus to the cytosol: a novel function for targeting by the PDZ domain of nNOS. *J. Biol. Chem.* **276**, 48262–48268.
42. Lin, X., Sun, B., Liang, M., Liang, Y. Y., Gast, A., Hildebrand, J. *et al.* (2003). Opposed regulation of corepressor CtBP by SUMOylation and PDZ binding. *Mol. Cell*, **11**, 1389–1396.
43. Dammer, E. B. & Sewer, M. B. (2008). Phosphorylation of CtBP1 by cAMP-dependent protein kinase modulates induction of CYP17 by stimulating partnering of CtBP1 and 2. *J. Biol. Chem.* **283**, 6925–6934.
44. Kitamura, N., Motoi, Y., Mori, A., Tatsumi, H., Nemoto, S., Miyoshi, H. *et al.* (2009). Suppressive role of C-terminal binding protein 1 in IL-4 synthesis in human T cells. *Biochem. Biophys. Res. Commun.* **382**, 326–330.
45. Bhambhani, C., Chang, J. L., Akey, D. L. & Cadigan, K. M. (2011). The oligomeric state of CtBP determines its role as a transcriptional co-activator and co-repressor of Wingless targets. *EMBO J.* **30**, 2031–2043.
46. Kajimura, S., Seale, P., Tomaru, T., Erdjument-Bromage, H., Cooper, M. P., Ruas, J. L. *et al.* (2008). Regulation of the brown and white fat gene programs through a PRDM16/CtBP transcriptional complex. *Genes Dev.* **22**, 1397–1409.
47. Perissi, V., Scafoglio, C., Zhang, J., Ohgi, K. A., Rose, D. W., Glass, C. K. & Rosenfeld, M. G. (2008). TBL1 and TBLR1 phosphorylation on regulated gene promoters overcomes dual CtBP and NCoR/SMRT transcriptional repression checkpoints. *Mol. Cell*, **29**, 755–766.
48. Purbey, P. K., Singh, S., Notani, D., Kumar, P. P., Limaye, A. S. & Galande, S. (2009). Acetylation-dependent interaction of SATB1 and CtBP1 mediates transcriptional repression by SATB1. *Mol. Cell. Biol.* **29**, 1321–1337.
49. Stern, M. D., Aihara, H., Roccaro, G. A., Cheung, L., Zhang, H., Negeri, D. & Nibu, Y. (2009). CtBP is required for proper development of peripheral nervous system in *Drosophila*. *Mech. Dev.* **126**, 68–79.
50. Wang, S. Y., Iordanov, M. & Zhang, Q. (2006). c-Jun NH2-terminal kinase promotes apoptosis by down-regulating the transcriptional co-repressor CtBP. *J. Biol. Chem.* **281**, 34810–34815.
51. Phelps, R. A., Chidester, S., Dehghanizadeh, S., Phelps, J., Sandoval, I. T., Rai, K. *et al.* (2009). A

two-step model for colon adenoma initiation and progression caused by APC loss. *Cell*, **137**, 623–634.
52. Tompa, P. (2012). Intrinsically disordered proteins: a 10-year recap. *Trends Biochem. Sci.* **37**, 509–516.
53. Moldoveanu, T., Gehring, K. & Green, D. R. (2008). Concerted multi-pronged attack by calpastatin to occlude the catalytic cleft of heterodimeric calpains. *Nature*, **456**, 404–408.
54. Hanna, R. A., Campbell, R. L. & Davies, P. L. (2008). Calcium-bound structure of calpain and its mechanism of inhibition by calpastatin. *Nature*, **456**, 409–412.
55. Sato, N., Kawahara, H., Toh-e, A. & Maeda, T. (2003). Phosphorelay-regulated degradation of the yeast Ssk1p response regulator by the ubiquitin-proteasome system. *Mol. Cell. Biol.* **23**, 6662–6671.
56. Ono, Y., Shimada, H., Sorimachi, H., Richard, I., Saido, T. C., Beckmann, J. S. *et al.* (1998). Functional defects of a muscle-specific calpain, p94, caused by mutations associated with limb-girdle muscular dystrophy type 2A. *J. Biol. Chem.* **273**, 17073–17078.
57. Almenar-Queralt, A., Gregorio, C. C. & Fowler, V. M. (1999). Tropomodulin assembles early in myofibrillogenesis in chick skeletal muscle: evidence that thin filaments rearrange to form striated myofibrils. *J. Cell Sci.* **112**, 1111–1123.
58. Pappas, C. T., Bhattacharya, N., Cooper, J. A. & Gregorio, C. C. (2008). Nebulin interacts with CapZ and regulates thin filament architecture within the Z-disc. *Mol. Biol. Cell*, **19**, 1837–1847.
59. Katoh, K., Asimenos, G. & Toh, H. (2009). Multiple alignment of DNA sequences with MAFFT. *Methods Mol. Biol.* **537**, 39–64.
60. Heger, A. & Holm, L. (2000). Rapid automatic detection and alignment of repeats in protein sequences. *Proteins*, **41**, 224–237.
61. duVerle, D., Takigawa, I., Ono, Y., Sorimachi, H. & Mamitsuka, H. (2010). CaMPDB: a resource for calpain and modulatory proteolysis. *Genome Inform.* **22**, 202–213.

PLOS ONE

# IQGAP1 Functions as a Modulator of Dishevelled Nuclear Localization in Wnt Signaling

**Toshiyasu Goto[1☯], Atsushi Sato[1☯], Masahiro Shimizu[1], Shungo Adachi[1], Kiyotoshi Satoh[1], Shun-ichiro Iemura[2], Tohru Natsume[2], Hiroshi Shibuya[1]***

**1** Department of Molecular Cell Biology, Medical Research Institute, Tokyo Medical and Dental University, Bunkyo-ku, Tokyo, Japan, **2** Biomedicinal Information Research Center, National Institutes of Advanced Industrial Science and Technology, Kohtoh-ku, Tokyo, Japan

## Abstract

Dishevelled (DVL) is a central factor in the Wnt signaling pathway, which is highly conserved among various organisms. DVL plays important roles in transcriptional activation in the nucleus, but the molecular mechanisms underlying their nuclear localization remain unclear. In the present study, we identified IQGAP1 as a regulator of DVL function. In *Xenopus* embryos, depletion of IQGAP1 reduced Wnt-induced nuclear accumulation of DVL, and expression of Wnt target genes during early embryogenesis. The domains in DVL and IQGAP1 that mediated their interaction are also required for their nuclear localization. Endogenous expression of Wnt target genes was reduced by depletion of IQGAP1 during early embryogenesis, but notably not by depletion of other IQGAP family genes. Moreover, expression of Wnt target genes caused by depletion of endogenous IQGAP1 could be rescued by expression of wild-type IQGAP1, but not IQGAP1 deleting DVL binding region. These results provide the first evidence that IQGAP1 functions as a modulator in the canonical Wnt signaling pathway.

**Citation:** Goto T, Sato A, Shimizu M, Adachi S, Satoh K, et al. (2013) IQGAP1 Functions as a Modulator of Dishevelled Nuclear Localization in Wnt Signaling. PLoS ONE 8(4): e60865. doi:10.1371/journal.pone.0060865

**Editor:** Masaru Katoh, National Cancer Center, Japan

**Received** February 5, 2013; **Accepted** March 4, 2013; **Published** April 5, 2013



**Funding:** This work was supported by Grants-in-Aid for scientific research from Japan Society for the Promotion of Science. The funders had no role in study design, data collection and analysis, decision to publish, or preparation of the manuscript.

**Competing Interests:** The authors have declared that no competing interests exist.

* E-mail: shibuya.mcb@mri.tmd.ac.jp

☯ These authors contributed equally to this work.

## Introduction

Wnt signaling plays important roles in multiple developmental events during embryogenesis [1], [2]. Canonical Wnt signaling is initiated by binding of the Wnt ligand to the cell-surface Frizzled and transmembrane LRP complex. This leads to the membrane recruitment and activation of Dishevelled (DVL), which inactivates the APC/Axin/GSK-3 complex in the cytoplasm, responsible for the degradation of ß-catenin [3], [4]. As a result, ß-catenin accumulates in the cytoplasm, translocates to the nucleus and associates with Tcf transcription factors, which activate the Wnt target genes [5], [6]. In *Xenopus*, Wnt signaling accompanied by ß-catenin nuclear localization at the dorsal side is an important for axis formation during early embryogenesis [7]. Ventral overexpression of *Xwnt-8*, *ß-catenin* and *DVL2* induces a secondary axis and promotes expression of Wnt target genes, such as *Siamois*, *Xnr3* and *Xtwn* [8]–[14].

There are three DVL isoforms, DVL1, DVL2 and DVL3 [15], [16], which are well-conserved among various organisms. Each isoform plays a similar role in the canonical Wnt pathway, but have different sensitivities to Wnt stimulation [17]. DVL contains three conserved regions known as the DIX, PDZ and DEP domains [18], [19]. Both the DIX and PDZ domains are necessary for canonical Wnt inactivation of ß-catenin degradation [20], [21]. In contrast, the DEP domain does not affect canonical signaling, but is involved in the planar cell polarity (PCP) pathway [21]–[23]. DVL plays an additional role in the Wnt signaling pathway, by localizing to the nucleus and binding a complex containing ß-catenin and Tcf, which in turn activates Wnt target genes in the nucleus [24]. The subcellular localization of DVL, either on the cell membrane or in the nucleus, is important for understanding its function in Wnt signaling.

IQGAP1 contains multiple protein-interacting domains: the CH (calponin homology) domain binds to F-actin, the WW domain binds to ERK2, the IQ repeat motifs bind to calmodulin and myosin light chain, and the Ras GAP-like domain binds to Cdc42 and Rac1 [25]–[32]. IQGAP1 is also known to bind to E-cadherin and ß-catenin, and is involved in cytoskeltal reorganization and cell adhesion [33], [34]. On the other hand, IQGAP1 stimulates ß-catenin-mediated transcriptional activation[34]. The subcellular localization of IQGAP1 varies in several cultured cells, and analysis of its domains indicates that IQGAP1 may be localized in the cytoplasm, cell membrane and nucleus [35]. These subcellular localizations are presumably linked to its cellular functions. There are also three isoforms of IQGAP: IQGAP1, IQGAP2 and IQGAP3. Their subcellular localizations suggest both similarities and differences in function [36]. Each isoform has a different role, and in some cases IQGAP1 has an opposite function to IQGAP2 [36], [37]. The *Xenopus xIQGAP1* and *xIQGAP2* genes have been isolated [38] and shown to be involved in cadherin-mediated cell adhesion [38], [39]. We also isolated *xIQGAP3* and have generated antisense morpholino oligonucleotides based on these sequences.

In the present study, we identified IQGAP1 as a novel DVL-binding protein. Binding between IQGAP1 and DVL2 mutually contributed to their nuclear localization. The depletion of

endogenous IQGAP1 in *Xenopus* embryos suppressed secondary axis induction and expression of Wnt target genes. These results reveal a novel role for IQGAP1 in modulating the subcellular localization and transcriptional activation of components of the Wnt signaling pathway.

## Materials and Methods

### Ethics statement

All animal experiments were performed under the ethical guidelines of Tokyo Medical and Dental University, and animal protocols were reviewed and approved by the animal welfare committee of the Tokyo Medical and Dental University.

### Plasmid construction

The human and *Xenopus DVL*, *IQGAP* isoforms were amplified by RT-PCR from cDNA templates prepared from HEK 293 cells and *Xenopus* embryos, respectively, and were subcloned into the pRK5 and pCS2+ vectors. Each truncated mutant was constructed by PCR and contained the following amino acid sequences. hDVL1-1: 1–486 aa, hDVL1-2: 476–671 aa, hIQGAP1-1: 1–669 aa, hIQGAP1-2: 631–951 aa, hIQGAP1-3: 631–1657 aa, hIQGAP1-4: 901–1060 aa, hIQGAP1-5: 1067–1154 aa, hIQGAP1-6: 1032–1116 aa, xDVL2-*Δ*IBR: 1–509 aa, xDVL2-IBR: 510–736 aa, xIQGAP1-*Δ*DBR: 1–856 and 1061–1657 aa, xIQGAP1-DBR: 857–1060 aa. We made GFP constructs of xDVL2, xIQGAP1 and their truncated mutants by conjugating with the GFP sequence at the C-terminus.

### Primers

The sequences of the primer pairs were as follows. In Figure S1, xDVL1: Forward 5′-CCAGCATAGCGAAGGTAGTA-3′; Reverse 5′-TACACCTTGCTCCCGATCTT-3′. xDVL2: Forward 5′-ATCTGACTGGCTGTGAGAAC-3′; Reverse 5′-TCAGACTCACTACCAGATCC-3′. xDVL3: Forward 5′-AAGTCTGGAGGAAGTGGAAG-3′; Reverse 5′-CATGCGGAAGGATTGTCTAC-3′. xIQGAP1: Forward 5′-CAGTGAACAGGAAGCAGATC-3′; Reverse 5′-TCAATGCTGTGTGTGTCTGC-3′. xIQGAP2: Forward 5′-CAGAAGAAAAGGGCTCCAAG-3′; Reverse 5′-AACATCTTCATCACGGCGAC-3′. xIQGAP3: Forward 5′-ACAGCCAACTTAGCATCGAG-3′; Reverse 5′-TGCTGTGTAATTGAGGGACG-3′. Ornithine decarboxylase (ODC): Forward 5′-GTCAATGATGGAGTGTATGGATC-3′; Reverse 5′-TCCATTCCGCTCTCCTGAGCAC-3′. IIn Figure S5, Glyceraldehyde-3-phosphate dehydrogenase (GAPDH): Forward 5′-GCCATCACTGCCACCCAGAAGACTG-3′; Reverse 5′-CATGAGGTCCACCACCCTGTTGCTG-3′. Axin2: Forward 5′-AACGACAGCGAGTTATCCAGCGACG-3′; Reverse 5′-ATGACACTGCTGATGGTGGTGGTGC-3′. TGFß2: Forward 5′-TGGCTTCACCATAAAGACAGGAACC-3′; Reverse 5′-CAGAAGTTGGCATTGTACCCTTTGG-3′. Mouse IQGAP1: Forwared 5′-AAGTTTGACGTGCCTGGTGA-3′; Reverse 5′-GGTATCTGTTCTTTGGGTCC-3′. xIQGAP1: Forward 5′-AGCTTGCAGATATGATGATG-3′; Reverse 5′-TTAGTCCACAGAGCTAATGATG-3′.

### Embryo handling and morpholino oligonucleotides

Capped mRNAs were synthesized from linearized vectors using the mMessage Machine kit (Ambion). The morpholino oligonucleotides (MO) (Gene Tools, LLC) used here were 5′-CCTCTTACCTCAGTTACAATTTATA-3′ (Control-MO), 5′-GTAGATGATTTTGGTCTCAGCCATG-3′ (*xDVL1*-MO), 5′-TCACTTTAGTCTCCGCCATTCTGCG-3′ (*xDVL2*-MO), 5′-GATGACCTTGGTCTCCCCCATAATT-3′ (*xDVL3*-MO), 5′-CATCGACTTCCTCCGAAACGGACAT-3′ (*xIQGAP1*-MO), 5′-GTCCTCATGGTTCATCCTGTTGCTG-3′ (*xIQGAP2*-MO), 5′-CCTCCGGCCTTACACTCCATTCCTG-3′ (*xIQGAP3*-MO). The specificity of each MO was confirmed by its ability to inhibit the translation of FLAG-tagged mRNAs containing the targeted site with or without 5-mismatched sequences. MO (10 ng) and FLAG-tagged mRNAs (100 pg) were co-injected with *β-globin-FLAG* mRNA (100 pg) as loading control into the animal poles of 4-cell stage embryos, and the injected animal caps were dissected at stage 10. Lysates from the animal caps were subjected to Western blotting with anti-FLAG antibody (M2, Sigma) (Fig. S1C).

MOs and mRNAs were injected into four animal blastomeres at the 4-cell stage for dissection of animal caps or into two dorsal or ventral blastomeres at the 4-cell-stage for quantitative RT-PCR analysis and observation of embryo phenotypes. Animal cap explants of the injected (10 pg mRNA of each GFP fused construct) embryos were dissected at the early gastrula stage (st.10), and fixed for DAPI staining as previously reported [40]. We counted the number of cell that has fluorescence signals. When the fluorescence signal overlapped with DAPI staining was similar and brighter than un-overlapped fluorescence signal in counted cells, we defined such cells as nuclear localized cells. If nuclear fluorescence signals were not clear, we used ImageJ software (NIH) and measured the strength of brightness of fluorescence signals to define nuclear localized signals or not. The ratio of nuclear localized cells in total counted cells was computed for every explant and the average of ratio was taken with six explants in 3 independent experiments. Dorsal or ventral sectors of the injected embryos were dissected at st.10, and total RNA was extracted for RT-PCR analysis. The cytoplasmic and nuclear fractions were prepared as described with modifications [41].

### RT-PCR analysis

Total RNA was prepared using TRIzol (Invitrogen). cDNA synthesis was carried out using Moloney murine leukemia virus reverse transcriptase (Invitrogen). Quantitative PCR was performed with an Applied Biosystems 7300 Real-Time PCR Cycler (ABI) using THUNDERBIRD SYBR qPCR Mix (TOYOBO). The sequences of the primer pairs were as follows. *Ornithine decarboxylase (ODC)*: Forward 5′-AAAATGGATGACTGCGAGATGGG-3′; Reverse 5′-AATGAAGATGCTGACTGGCAAAAC-3′. *Siamois*: Forward 5′-CTGTCCTACAAGAGACTCTG-3′; Reverse 5′-TGTTGACTGCAGACTGTTGA-3′. *Xnr3*: Forward 5′-CTTCTGCACTAGATTCTG-3′; Reverse 5′-CAGCTTCTGGCCAAGACT-3′. *Xtwn*: Forward 5′-AACCCAAGAAGGCGACACTATC-3′; Reverse 5′-GTGCCGATGGTAGGAAATGATC-3′. *Xenopus* embryonic *ODC* was used for normalization of cDNA samples.

### Antibodies and cell lines

The following antibodies were used for immunoprecipitation and/or Western blotting analysis: Horseradish peroxidase conjugated anti-mouse IgG (GE); Horseradish peroxidase conjugated anti-rabbit IgG (GE); anti-FLAG (M2 and F7425, Sigma); anti-MYC (9B11, Cell Signaling); anti-DVL1 (3F12 and Q-25, Santa Cruz); anti-IQGAP1 (H-109, Santa Cruz); anti-beta-tubulin (sc-58884, Santa Cruz); anti-histone-H3 (sc-10809, Santa Cruz). We used following cell lines: HEK 293 cells [42], HEK 293T cells [43], NIH3T3 cells [43], L cells (CRL-2648, ATCC), L Wnt3A cells (CRL-2647, ATCC). Recombinant human Wnt3A (R&D Systems; 20 ng/ml) or four day Wnt-3A conditioned medium from L-Wnt-3A cells was used for Wnt stimulation of cultured

cells. The growth medium for each cell type is described by American Type Culture Collection.

### Protein identification by LC-MS/MS analysis

FLAG-human DVL1 was expressed in HEK 293 cells, and DVL1 and associated proteins were recovered from cell extracts by immunoprecipitation with anti-FLAG antibody. The DVL1-associated complexes were digested with *Axhromobacter* protease I, and the resulting peptides were analyzed using a nanoscale LC-MS/MS system, as described previously [44].

## Results

### IQGAP associates with DVL

To identify novel proteins that may bind to DVL, we performed a high-throughput analysis of proteins that co-immunoprecipitated with mouse DVL1 in HEK 293 cells using direct nanoflow liquid chromatography-coupled tandem mass spectrometry [44]. We identified several known DVL-binding proteins, such as CK1 [45], CK2 [46], Strabismus [47], Par1 [48], Axin [49] and PP2C [50]. In addition, we identified IQGAP1 as a candidate protein that may physically interact with DVL1. An interaction between ectopically expressed IQGAP1 and DVL1 was confirmed in HEK 293 cells (Fig. 1A). Immunoprecipitation analysis using each protein antibody also confirmed the existence of an endogenous IQGAP1 and DVL1 complex in HEK 293T cells, and their interaction was increased by Wnt stimulation (Fig. 1B). In vertebrates, three isoforms of IQGAP and DVL have been identified: IQGAP1, IQGAP2 and IQGAP3, and DVL1, DVL2 and DVL3. We confirmed that each IQGAP isoform also bound to each DVL isoform (Fig. 1C-1E). To determine the region in IQGAP1 responsible for binding to DVL1, several truncated mutants of IQGAP1 were examined in co-precipitation assays. We found that the region between the C-terminal IQ repeat domain and the N-terminal Ras GAP-like domain of IQGAP1 (termed DBR; Dishevelled Binding Region) was responsible for binding to DVL1 (Fig. 1F and 1G) Conversely, the C-terminus of DVL1 (termed IBR; IQGAP Binding Region) is necessary for binding to IQGAP1 (Fig. 1H and 1I). Both the IBR and DBR are well-conserved among the three DVL and IQGAP isoforms, respectively. The amino acid sequence similarities of IBR and DBR among the three DVL and IQGAP isoforms were as follows, the similarity of IBR between DVL1 and DVL2 is 47.1%; the similarity of IBR between DVL1 and DVL3 is 55.7%; the similarity of IBR between DVL2 and DVL3 is 53.7%; the similarity of DBR between IQGAP1 and IQGAP2 is 82.4%; the similarity of DBR between IQGAP1 and IQGAP3 is 76.8%; the similarity of DBR between IQGAP2 and IQGAP3 is 72.8%. We conclude that IQGAP1 can associate with DVL in mammalian cells.

### IQGAP1 determines the nuclear localization of DVL

Whereas membrane-localized DVL functions to inhibit degradation of cytoplasmic ß-catenin in the canonical Wnt pathway [20], [21], nuclear-localized DVL is required, together with nuclear ß-catenin, for transactivation of the downstream targets of Wnt signaling [24]. To analyze DVL and IQGAP1 functions, we used the systems of *Xenopus* embryos. All isoforms of DVL and IQGAP are conserved well among vertebrates. The transcripts of their *Xenopus* homologues were expressed during early embryonic stages and were equivalently expressed at early gastrula stages (Fig. S1A and S1B). We subcloned their cDNA and generated their antisense morpholino oligo nucleotides (Fig. S1C). To examine how IQGAP affects DVL localization in Wnt signaling, we investigated the subcellular distribution of DVL fused to green fluorescent protein (GFP) in *Xenopus* embryonic cells. Fluorescence produced by the DVL2 (xDVL2)-GFP fusion appeared as a punctate pattern in the cytoplasm (Fig. 2A, left panel). DVL has been reported to be recruited to the plasma membrane by the Frizzled receptors in the Wnt pathway [21]. We confirmed that xDVL2-GFP accumulated in the plasma membrane when co-expressed with *Xenopus frizzled 7* (*Xfz7*) (Fig. 2A, center panel). Depletion of xIQGAP1 by antisense morpholino oligonucleotides (*xIQGAP1*-MO) did not affect the membrane localization of xDVL2-GFP (Fig. 2A, right panel). These results suggest that xIQGAP1 is not involved in the plasma membrane localization of xDVL2.

Stimulation by Wnt ligands is known to increase the nuclear localization of DVL [40]. When *xDVL2-GFP* was co-expressed with *Xwnt-8* in animal cap cells, nuclear GFP fluorescence was increased (Fig. 2B, third and fourth panels, 2D, lanes 1, 3), whereas GFP was mainly localized in the cytoplasm with or without *Xwnt-8* (Fig. 2B, first and second panels, 2C). However, injection of *xIQGAP1*-MO decreased nuclear fluorescence generated by co-expression of *xDVL2-GFP* and *Xwnt-8* (Fig. 2B, fifth and sixth panels, 2D, lanes 3, 4). We also confirmed that the amounts of xDVL2-MYC protein in the nuclear fractions of animal cap cells were reduced by depletion of xIQGAP1 (Fig. 2E). Expression of xIQGAP1-GFP resulted in fluorescence localized mainly to the cytoplasm, but nuclear fluorescence was increased by co-expression of *Xwnt-8* (Fig. 3A, first and second panels, 3B, lanes 1,3). Depletion of xDVL2 led to a decrease in nuclear fluorescence generated by the co-expression of *xIQGAP1-GFP* and *Xwnt-8* (Fig. 3B, lanes 3, 4). Moreover, we found that depletion of all three xDVLs (xDVL1, xDVL2 and xDVL3) reduced severely the nuclear localization of xIQGAP1-GFP in Wnt-stimulated cells (Fig. 3A, third and fourth panels, 3C, lanes 3, 4 and 3D). These results suggest that xIQGAP1 and xDVL2 play a crucial role in each other nuclear accumulation, depending on Wnt signaling.

We next examined whether a physical interaction between xIQGAP1 and xDVL2 is required for their nuclear localization. We generated a fusion of GFP to xDVL2-*Δ*IBR, a truncated version of xDVL2 lacking the IBR domain, and observed a punctate fluorescence pattern in the cytoplasm, similar to that seen with xDVL2-GFP (Fig. S2A). The proportion of fluorescence found in the nucleus was also similar to xDVL2-GFP (Fig. S2B). However, co-expression of *Xwnt-8* did not alter the proportion of GFP fluorescence found in the nucleus, (Fig. S2B), suggesting that the ability of xIQGAP1 to promote nuclear localization of xDVL2 requires the IBR domain in xDVL2. Consistent with this, a fusion of just the IBR domain to GFP (xDVL2-IBR-GFP) was localized predominantly in the nucleus (Fig. S2A and S2C). We next fused GFP to xIQGAP1-*Δ*DBR, which deletes the DBR domain of xIQGAP1. This xIQGAP1-*Δ*DBR-GFP fusion was also localized mainly in the cytoplasm (Fig. S2A), and the proportion of fluorescence found in the nucleus was less than that observed with full-length xIQGAP1-GFP (Fig. S2D). Co-expression of *Xwnt-8* also did not affect the nuclear localization of xIQGAP1-*Δ*DBR-GFP (Fig. S2D). A fusion of just the DBR domain to GFP (xIQGAP1-DBR-GFP) was localized mainly in the nucleus (Fig. S2A and S2E). We further investigated the effects of over-expression of xIQGAP1 or xDVL2 on the nuclear localization of xDVL2-GFP or xIQGAP1-GFP, respectively. Nuclear localization of xDVL2-GFP was increased by the expression of *xIQGAP1* and *xIQGAP1-DBR* (Fig. S3A). Meanwhile, expression of *xIQGAP1-ΔDBR* suppressed the nuclear localization of xDVL2-GFP induced by co-expression of *Xwnt-8* (Fig. S3A). In contrast, the nuclear localization of xIQGAP1-GFP was not affected by the expression

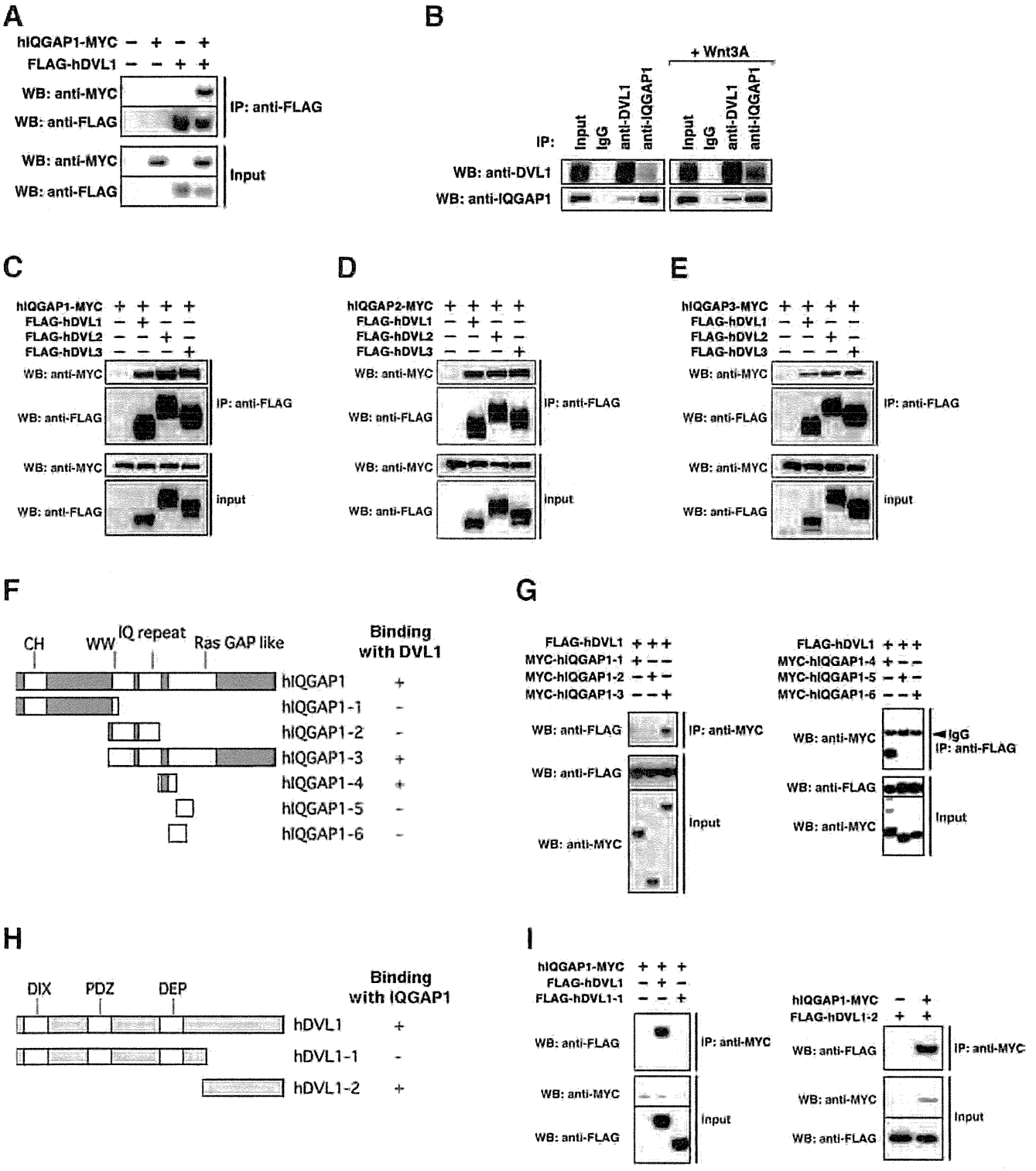


**Figure 1. IQGAP associates with DVL.** (**A**) Interaction between ectopically-expressed hIQGAP1 and hDVL1 in HEK 293 cells. Immunoprecipitates (IP) obtained using anti-FLAG antibody were subjected to Western blotting (WB) with the indicated antibodies. +, present; -, absent. (**B**) Interaction between endogenous hIQGAP1 and hDVL1 in HEK 293T cells. The cultured cells were stimulated with recombinant human Wnt3A for 6 hours (right panels). (**C–E**) Interaction between ectopically-expressed hIQGAP1, hIQGAP2, hIQGAP3 and hDVL isoforms in HEK 293T cells. (C) hIQGAP1. (D) hIQGAP2. (E) hIQGAP3. (**F**) A schematic of the domains of hIQGAP1 and truncated constructs. (**G**) Interactions between ectopically-expressed hDVL1 and truncated hIQGAP1 constructs. (**H**) Interactions among ectopically-expressed hIQGAP1 and truncated hDVL1 constructs. (**I**) A schematic of the domains of hDVL1 and truncated constructs.

doi:10.1371/journal.pone.0060865.g001

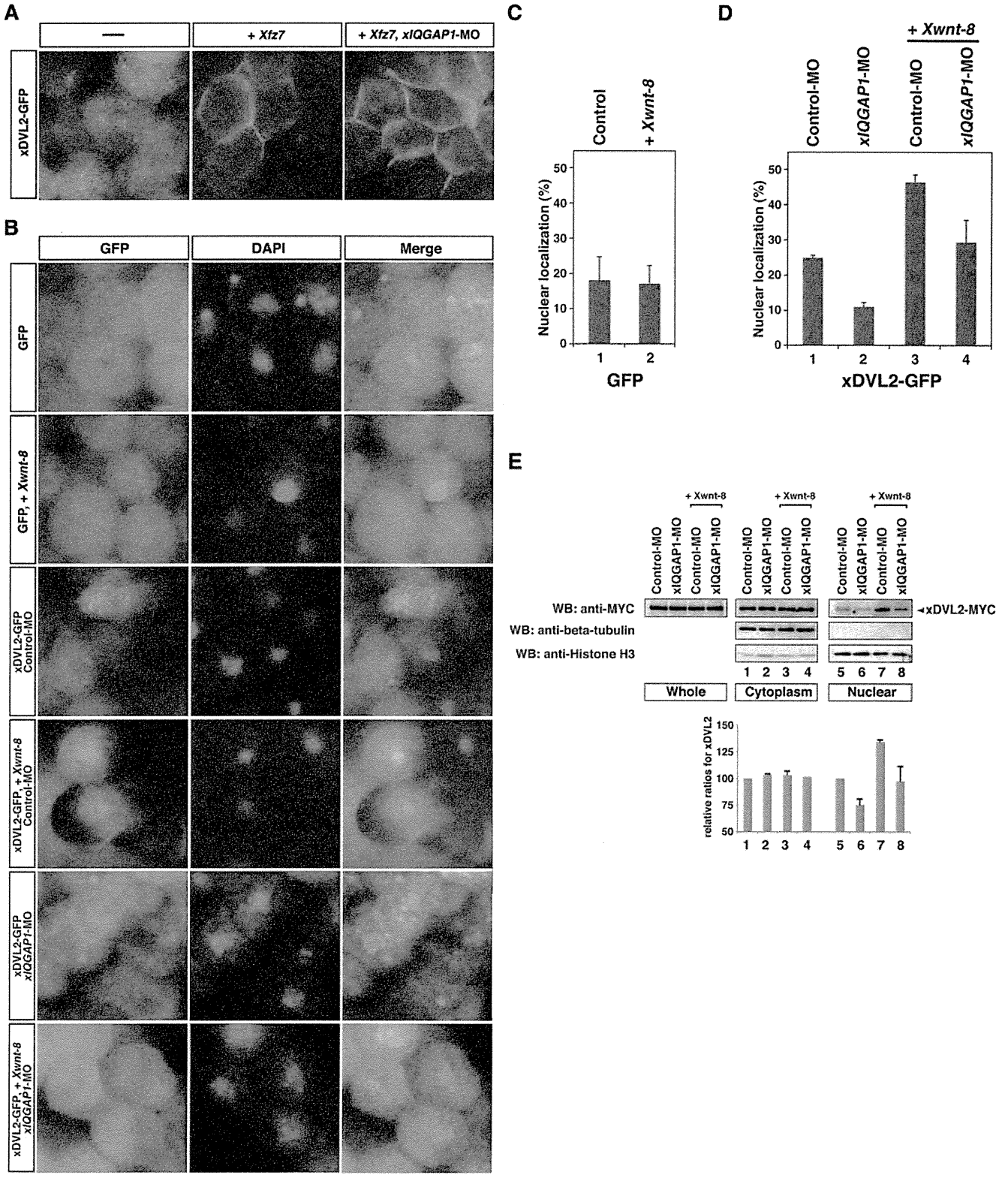


**Figure 2. Localization of xDVL2-GFP.** (**a,b**) Localization of xDVL2-GFP in *Xenopus* animal cap cells at stage 10. (**A**) xDvl2-GFP localized in punctate structures in the cytoplasm (left). Over-expression of *Xfz7* recruited xDVL2-GFP to the plasma membrane (center). *xIQGAP1*-MO did not affect the membrane localization of xDVL2-GFP induced by *Xfz7* (right). (**B**) Nuclear localization of GFP and xDVL2-GFP caused by over-expression of *Xwnt-8* and *xIQGAP1*-MO. GFP signals (left). DAPI staining of animal cap cells (center). Merge (right). (**C, D**) The ratio of cells that had nuclear fluorescence signals. The average of ratio was taken with six explants in 3 independent experiments (See Materials and Methods). Error bars represent standard deviation of the mean with six explants. Statistical significance was determined by Student's *t*-test. (**C**) The ratio of GFP localized in the nucleus in cells. *Xwnt-8* was co-injected in lanes 2. Lane 1: n = 291, 18.2%, lane 2: n = 320, 17.2%. P>0.1 [between lane 1 and lane 2]. (**D**) The ratio of xDVL2-GFP localized in the nucleus in cells injected with *xIQGAP1*-MO. *Xwnt-8* was co-injected in lanes 3 and 4. Lane 1: n = 918, 26.0%, lane 2: n = 1694, 11.0%, lane 3: n = 263,

46.4%, lane 4: n = 477, 29.4%. P<0.01 [between lane 1 and lane 2], P<0.01 [between lane 3 and lane 4]. (**E**) Cytoplasmic and nuclear distribution of xDVL2, xIQGAP1 and ß-catenin in animal cap cells. MYC-tagged *xDVL2* mRNA (100 pg) was injected into the animal poles of 4-cell stage embryos, and the injected animal caps were dissected at stage 10. Lysates from the animal caps were fractionated and subjected to Western blotting with indicated antibodies. Each relative intensity was measured by ImageJ, and its relative ratio was calculated against Input with beta-tubulin for cytoplasm or with Histone H3 for nuclear. Error bars represent standard deviation of the mean in three experiments. Statistical significance was determined by Student's *t*-test. P<0.1 [between lane 5 and lane 6], P<0.1 [between lane 7 and lane 8].
doi:10.1371/journal.pone.0060865.g002

of xDVL2 or xDVL2-IBR (Fig. S3B). However, *xDVL2-ΔIBR* suppressed the nuclear localization of xDVL2-GFP induced by co-expression of *Xwnt-8* (Fig. S3B). Moreover, immunoprecipitation experiments showed that Wnt stimulation increased the interaction between xDVL2 and xIQGAP1 in HEK 293T cells (Fig. 3E). Taken together, these results suggest that a physical interaction between xDVL2 and xIQGAP1 is required for their nuclear localization induced by the canonical Wnt signaling pathway.

### xIQGAP1 is necessary for the canonical Wnt pathway

To determine whether xIQGAP1 is also involved in the canonical Wnt pathway during early development, we investigated the effects of *xIQGAP1* on the transactivation of Wnt target genes and the secondary axis induction. Dorsal injection of an antisense morpholino oligonucleotide against xIQGAP1 (*xIQGAP1*-MO) reduced endogenous transcripts of the Wnt signal target genes *Siamois*, *Xnr3* and *Xtwn* (Fig. 4A). When *xDVL2*, *Xwnt-8* or *β-catenin* mRNA was injected into the ventral sides of four-cell embryos, a secondary axis was formed and Wnt signal target genes were induced. The induction of the partial secondary axis and Wnt target genes induced by *Xwnt-8* was also suppressed by the depletion of xIQGAP1 (Fig. 4B–4D). Dorsal overexpression of *xIQGAP1* mRNA increased expression of Wnt target genes (Fig. 4E). On the other hand, the overexpression or depletion of *xIQGAP2* showed opposite effects for Wnt target gene expression (Fig. 4A, 4D and 4E). *xIQGAP3* showed ambiguous effects on Wnt target gene expression, especially expression of *Siamois* (Fig. 4A, 4D and 4E). However, depletions of either xIQGAP2 or xIQGAP3 did not alter the partial secondary axis induction by *Xwnt-8* (Fig. 4B and 4C). These results suggest that xIQGAP1 is necessary for Wnt-related early embryogenesis in a subtype-specific manner.

We also found that the suppressions of induction of Wnt target genes and partial secondary axis by *xIQGAP1*-MO were rescued by expression of wild-type *xIQGAP1*, but not by either *xIQGAP1-ΔDBR* or *-DBR* (Fig. 4F, 4G, S4A–S4D). However, depletion of xIQGAP1 did not affect the secondary axis formation induced by *Simaois*, which is one of the Wnt signal target genes (Fig. 4H). Moreover, we also observed the reduction of endogenous IQGAP1 by the siRNA (siIQGAP1) suppressed the expression of Wnt target genes induced by Wnt3A stimulation in cultured cells (Fig. S5A). These results suggest that xIQGAP1 functions as an intermediate molecule in the canonical Wnt signaling pathway in early development promoting the nuclear localization of xDVL2.

### The IQGAP binding region of xDVL2 is important for canonical Wnt signaling

To further confirm whether the binding between IQGAP1 and DVL is critical in the canonical Wnt pathway during early development, we investigated the effects of *xDVL* mutants on the transactivation of Wnt target genes and secondary axis induction. Similar to our previous observation that injection of *xDVL2*-MO did not affect severely nuclear localization of xIQGAP1 (Fig. 3B), we also observed no reduction in Wnt target gene expression induced at the ventral side by *Xwnt-8* when *xDVL2*-MO was co-injected (Fig. 5A). However, depletion of all three xDVLs reduced nuclear localization of xIQGAP1, expression of the Wnt target genes and suppressed formation of the secondary axis induced by *Xwnt-8* or *β-catenin* (Fig. 3C, 3D, 5B, and 5C). These results suggest that three xDVL genes act redundantly in the canonical Wnt signal pathway. Suppression of secondary axis formation and Wnt target gene expression caused by depletion of all three xDVLs could be rescued by co-expression of wild-type *xDVL2*, but only weakly by *xDVL2-ΔIBR* and barely by *xDVL2-IBR* (Fig. 5B, and 5C). Moreover, co-expression of *xIQGAP1-DBR* reduced the expression of Wnt target genes induced by *Xwnt-8*, *xDVL2* or *β-catenin* in *Xenopus* embryos (Fig. 5D, S6A and S6B), and the expression of xIQGAP1-DBR in cultured cells reduced the expression of Wnt target gene induced by Wnt3A (Fig. S5B). These results support the idea that binding between xDVL2 and xIQGAP1 plays important roles for canonical Wnt signaling.

## Discussion

In the present studies, we show that IQGAP1 is necessary for the nuclear localization of DVL in the canonical Wnt signaling pathway. Previous studies have shown that nuclear localization of DVL is necessary for the sequential activation of Wnt target genes [24], [40]. It has also been shown that the nuclear localization signal (NLS) located between the PDZ and DEP domain of xDVL2, and the nuclear export signal (NES) located at the C-terminus are important for the nuclear localization and transcriptional activation of Wnt target genes [40]. Interestingly, we observed that xDVL2-IBR, a truncated protein consisting of just the IQGAP-binding region from the C-terminus of xDVL2, localized predominantly in the nucleus, even though this region contains an NES and not an NLS. Moreover, the nuclear localization of xDVL2-ΔIBR-GFP, which contains an NLS, but not an NES, did not increase with Wnt-8 stimulation any longer. Although our findings suggest a new molecular mechanism mediating xIQGAP1-dependent nuclear localization of xDVL2, we could not positively state that our findings is independent of the NLS or NES motifs within DVL2. Further studies need to clarify the inconsistencies using same mutants.

In the canonical Wnt pathway, DVL is necessary for both the inactivation of ß-catenin degradation in cytoplasm[21] and the activation of Wnt target genes by forming a complex containing ß-catenin and Tcf in nuclei [24]. In the present study, we have shown that IQGAP1 interacted with DVL and that the depletion of IQGAP1 reduced the nuclear localization of DVL, while IQGAP1 did not affect on the membrane localization of DVL required for ß-catenin stability in cytoplasm. These results suggest that IQGAP1 plays a role in the nuclear translocation of DVL in the canonical Wnt pathway.

We showed that the nuclear localization of xIQGAP1 and xDVL2 were increased by Wnt stimulation. In contrast, the nuclear localization of xDVL2-ΔIBR-GFP and xIQGAP1-ΔDBR-GFP did not increase with Wnt stimulation, while over-expression of *xDVL2-ΔIBR* or *xIQGAP1-ΔDBR* interfered with the nuclear localization of xIQGAP1-GFP or xDVL2-GFP induced by Wnt stimulation, respectively. Reduced expression of Wnt target genes due to depletion of endogenous xIQGAP1 or xDVLs was barely or weakly rescued by expression of *xIQGAP1-ΔDBR* or *xDVL2-ΔIBR*, respectively. Conversely, xDVL2-IBR-GFP and xIQGAP1-DBR-